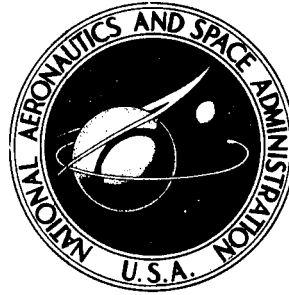NASA TECHNICAL NOTE

NASA TN D-6382

EXPERIMENTAL AND ANALYTICAL INVESTIGATION OF FAST NORMAL SHOCK POSITION CONTROLS FOR A MACH 2.5 MIXED-COMPRESSION INLET

by George H. Neiner, Michael J. Crosby, and Gary L. Cole

Lewis Research Center
Cleveland, Ohio 44135

CONTENTS

APPENDIXES

EXPERIMENTAL AND ANALYTICAL INVESTIGATION OF FAST NORMAL SHOCK

POSITION CONTROLS FOR A MACH 2.5 MIXED-COMPRESSION INLET

by George H. Neiner, Michael J. Crosby, and Gary L. Cole

Lewis Research Center

SUMMARY

Results of a normal shock position controls program for a supersonic inlet are presented. It was desirable to investigate normal shock position controls where the inlet overboard bypass-door system dynamics was not the limiting factor in the performance of the normal shock control system. The controls used a 110-hertz bypass-door system and 250-hertz pressure measurement system. The inherent inlet dynamics showed a resonance at 55 hertz. An analytical program was conducted first, followed by experimental tests. The inlet used for testing was a Mach 2.5 design axisymmetric, mixed-compression inlet having 60 percent internal supersonic area contraction at the design Mach number. The tests were conducted in the Lewis 10- by 10-Foot Supersonic Wind Tunnel. The inlet using various control systems was subjected to inlet diffuser exit airflow disturbances over the range of frequencies from 0 to 140 hertz. The controls investigation was conducted with three different inlet terminations. The terminations consisted of a long pipe with a choked exit plug, a choked orifice plate close to the diffuser exit station, and a J85-13 turbojet engine. The best control was a two-loop control with electronic compensation. With this control, the disturbance induced shock motion was reduced relative to its open-loop value over a frequency range from 0 to 40 hertz. At 1 hertz the disturbance-induced shock motion was reduced by a factor of more than 10:1 relative to its open-loop value. Although the amplitude of shock motion of the controlled inlet was reduced over a frequency range from 0 to 40 hertz, it was amplified above the open loop in the region of an inherent inlet resonance at 55 hertz.

INTRODUCTION

The basic function of the supersonic inlet is to change the kinetic energy of the air entering the inlet into a static pressure rise by slowing down the air velocity. In doing

this the inlet should maintain high total pressure recovery and low distortion of the pressure profile at the diffuser exit. In general, total pressure recovery increases and distortion decreases at the diffuser exit of a mixed-compression inlet as the normal shock is moved closer to the throat. Thus a shock operating point near the inlet throat is desirable. But airflow disturbances from within or external to the inlet can cause the shock to move from its operating point. A displacement in the upstream direction could result in an inlet unstart. A downstream displacement might result in the loss of engine performance because of lower pressure recovery or a compressor stall due to increased distortion. Any of these events are undesirable and can usually be avoided or at least minimized by supplying the inlet with a normal shock control system.

A common way of regulating the inlet normal shock against downstream disturbances is to manipulate overboard bypass doors near the diffuser exit to match inlet airflow to engine airflow requirements. Other experimental work in the area of inlet open-loop dynamics and the selection of signals for control of normal shock position are discussed in references 1 to 3. Additional experimental investigations for normal shock position control are discussed in references 3 to 7. In the past relatively slow bypass doors (10-Hz bandwidth) have been used. It is possible, however, that high-frequency disturbances may exist (such as might be generated by a turbofan) that could not be controlled by such slow bypass doors. It was the intent of this investigation, therefore, to design and test a normal shock position control system whose dynamic performance was not limited by the dynamics of the inlet bypass system. The frequency response of normal shock position to a downstream airflow disturbance for the inlet used in this investigation exhibited a pronounced resonance at 55 hertz. The inlet bypass-door position control system had a corner frequency of 110 hertz. Internal inlet pressure signals downstream of the normal shock were used to indicate shock position and were fed back to manipulate bypass-door position.

This report includes a discussion of the analytical program that was carried out initially to determine what control types should be investigated experimentally. Both analytical and experimental data are presented and discussed for the most promising control systems that were investigated. The experimental program was conducted in the 10- by 10-Foot Supersonic Wind Tunnel at the Lewis Research Center. Tests were conducted with three different inlet terminations. One was a long pipe with a choked plug exit; this configuration introduced a large volume between the diffuser exit and the choked plug exit. A second termination consisted of a choked orifice plate near the diffuser exit. The third termination was a turbojet engine. The various normal shock controllers were tested by subjecting the controlled inlet to sinusoidal downstream airflow disturbances over a frequency range from 0 to 140 hertz.

APPARATUS

Inlet

Inlet physical description. - The inlet selected for this investigation was an axisymmetric mixed-compression type with a translating centerbody. Sixty percent of the total supersonic area contraction occurred internally at the design Mach number of 2.5. The cowl lip diameter of the inlet was 47.3 centimeters. The inlet had a capture area of 1760 square centimeters, and a design capture corrected airflow of 16.2 kilograms per second.

Figure 1 is an isometric drawing of the inlet. The translating centerbody is hydraulically actuated and electronically controlled. The aft portion of the diffuser is divided by three struts which extend aft to the compressor face station. In each of the three compartments are located two overboard bypass doors. The six bypass doors were designed to pass 88 percent of the design inlet capture airflow. Each door is hydraulically actuated and electronically controlled.

Boundary-layer bleed holes are located in the vicinity of the geometric throat on both the cowl and centerbody surfaces. For this investigation bleed configuration I (see ref. 8) was used during engine tests and configuration II during tests with the long pipe and choked orifice plate terminations. The cowl bleed exits are shown in figure 1. The centerbody bleed flow was ducted through two of the three centerbody struts to the free stream. Vortex generators were used on the centerbody of the inlet during the long pipe and choked orifice plate tests. During tests with the engine, vortex generators were also used on the cowl to help reduce distortion at the diffuser exit. The overboard bypass and engine cooling flows are also shown in the figure. The engine cooling bypass flow was used to cool the engine when the inlet was terminated with the engine. At design conditions it passed 3 percent of the inlet airflow.

The dynamic responses of the inlet's normal shock and various internal pressures to upstream and downstream sinusoidal airflow disturbances are described in reference 8. Aerodynamic design and steady-state performance of the inlet are described in references 9 and 10.

Inlet terminations. - Three inlet terminations were used for this investigation; they are shown schematically in figure 2. The terminations were installed in a 63.5-centimeter cylindrical nacelle. The first termination was a long pipe, choked at the model exit plug and shown in figure 2(a). The length of this long pipe was 236 centimeters, while its diameter was 38.0 centimeters. The exit plug area was remotely adjustable. The second termination consisted of the choked orifice plate also shown in figure 2(a). It was positioned 146.5 centimeters downstream of the cowl lip. The flow area of the choked orifice plate was 653 square centimeters. When the choked orifice plate was installed, the model exit plug was retracted in the downstream direction to cause a

choked flow condition at the plate. The third termination was the J85-13 turbojet engine as shown in figure 2(b). Figure 3 is a photograph of the model installed in the 10- by 10-Foot Supersonic Wind Tunnel.

Inlet transfer function. - Analytical open-loop inlet dynamics were used in determining the controllers before the controls investigation. The experimental inlet dynamic data, which were taken during the analytical controls design activity, were not available for designing the controllers. These experimental data are presented in reference 8. They are used in part herein as reference information to show the effectiveness of the control system and also to show a comparison with the analytical responses.

A signal flow block diagram of the inlet is shown in figure 4. The inlet dynamic signals of interest for this investigation are shock position X, throat exit static pressure P_{56}, and diffuser exit static pressure P_{92}. These symbols as well as the rest of the symbols appearing in the report are defined in appendix A. The transfer functions which relate these signals to a downstream airflow disturbance W_{bd} are indicated in figure 4. The transfer functions consist of two types of factors: the steady-state gain, which is represented by K_{92}, K_{56}, and K_x; and the dynamic term (the frequency dependent part), which is represented by G_{92}, G_{56}, and G_x. The open-loop dynamic terms have been normalized so that their low-frequency magnitude is equal to one.

Inlet steady-state gains: Table I lists the values of steady-state gain for X, P_{56}, and P_{92} related to a downstream airflow disturbance W_{bd} for all three inlet terminations. Ideally, if the same operating point and disturbance size were used for all three inlet terminations all three gains would be the same. However, because the system is nonlinear and the same operating points and disturbance magnitudes were not used for testing with each inlet termination, a particular gain had different values depending on which inlet termination was used.

TABLE I. - STEADY-STATE GAIN OF INLET SIGNALS

FOR THE DIFFERENT INLET TERMINATIONS

Ratio of variables	Steady-state gains	Inlet terminations			Units
		Long pipe	Choked orifice plate	Engine	
$\Delta X/\Delta W_{bd}$	$K_{92}K_{56}K_x$	12	16	10	$\dfrac{cm}{kg/sec}$
$\Delta P_{56}/\Delta W_{bd}$	$K_{92}K_{56}$	1.2	1.5	1.0	$\dfrac{N/cm^2}{kg/sec}$
$\Delta P_{92}/\Delta W_{bd}$	K_{92}	.85	1.1	.7	$\dfrac{N/cm^2}{kg/sec}$

4

The experimental frequency responses of the dynamic terms of the inlet transfer functions (X, P_{56}, and P_{92} to W_{bd}), as illustrative of the nature of the dynamics of the process to be controlled, will be presented next in the form of normalized Bode plots.

Shock position dynamics: In terms of the block diagram shown in figure 4, the transfer function relating shock position to the downstream airflow disturbance is

$$\frac{X}{W_{bd}} = K_{92}G_{92}K_{56}G_{56}K_x G_x$$

The open-loop normalized response of shock position to a downstream airflow disturbance W_{bd} is shown in figure 5. The curves represent shock position response to a downstream airflow disturbance with the inlet terminated with the long pipe, with the choked orifice plate, and J85-13 engine, respectively. The curves of figure 5 also represent the normalized open-loop frequency response, namely,

$$\left.\frac{X}{W_{bd}}\right|_N = G_{92}G_{56}G_x$$

The phase shift of the three curves of figure 5 for the downstream disturbance are quite similar. A dead time dominates the phase characteristics. The 180° phase shift occurs at approximately 60 hertz for all three terminations.

The amplitude ratio curves for the three terminations are markedly different. The long pipe with its large downstream volume, exhibits a low-frequency first-order corner. However, in the vicinity of the frequency at which 180° phase shift occurs, the long pipe resonates such that its amplitude ratio is near that of both the choked orifice plate and engine configurations. Thus, from a stability point of view for a closed-loop system, all three terminations present the problem of a large amplitude ratio at the frequency at which 180° phase lag occurs.

Throat exit static pressure dynamics: In terms of the block diagram of figure 4, the transfer function relating P_{56} to the downstream airflow disturbance is

$$\frac{P_{56}}{W_{bd}} = K_{92}G_{92}K_{56}G_{56}$$

The normalized open-loop response of throat exit static pressure P_{56} to the downstream airflow disturbance W_{bd} is

$$\left.\frac{P_{56}}{W_{bd}}\right|_N = G_{92}G_{56}$$

The curves of figure 6 represent $P_{56}/W_{bd}|_N$ with the inlet terminated with the long pipe, the choked orifice plate, and the J85-13 engine. The P_{56} responses are quite similar to the shock position responses except that they exhibit somewhat less phase lag.

Diffuser exit static pressure dynamics: In terms of the block diagram notation in figure 4 the transfer function relating P_{92} to the downstream airflow disturbance is

$$\frac{P_{92}}{W_{bd}} = K_{92}G_{92}$$

The curves of figure 7 are the normalized open-loop response of P_{92} to the downstream airflow disturbance for the long pipe, choked orifice plate, and engine terminations. The normalized open-loop response is

$$\left.\frac{P_{92}}{W_{bd}}\right|_N = G_{92}$$

A most important characteristic of the diffuser exit pressure response is the relatively small phase lag in the vicinity of the resonance. Since this pressure is near the source of the downstream airflow disturbance, it is not characterized by the duct dead time. Thus, this signal can serve as an anticipatory function for the control of shock position against downstream airflow disturbances.

Dynamic Pressure Transducers

Figures 8 and 9 indicate the location of static pressure taps connected to the dynamic strain-gage pressure transducers used in this investigation. The throat exit static pressure P_{56} and diffuser exit static pressure P_{92} were used as feedback control signals. The pressure signals are identified by their model station numbers. These numbers are the distances in centimeters aft of the cowl lip. Figure 9 shows an enlarged view of the throat region and the location of the throat static pressure taps. Looking downstream, all the static pressure taps were essentially in line, 30° counterclockwise from top center of the inlet. The transducers were close-coupled within 3 to 4 centimeters of the taps to insure adequate dynamic response.

The transfer functions h_{56} and h_{92} of figure 4 represent the dynamics of the transducers and the tubes connecting the taps and transducers for P_{56} and P_{92}, respectively. The normalized frequency response curves representing h_{56} and h_{92} are shown in figure 10. The P_{56} and P_{92} frequency response data were corrected to account for the dynamics in measuring the pressures. The amplified output of the transducers had a gain of $1.45 \text{ V}/(\text{N}/\text{cm}^2)$.

Overboard Bypass-Door System

During the test program three symmetrically located inlet overboard bypass doors were used to generate downstream airflow disturbances, and the remaining three doors were used for control.

A bypass-door assembly is shown in figure 11. Each door consisted of a hydraulically actuated sliding plate, with four slots, which were controlled by a position servomechanism. Figure 12 is a schematic of the bypass-door installation. The servoamplifier was designed at Lewis for high-response electrohydraulic servosystems. Details of the servoamplifier are presented in reference 11. A detailed discussion of the bypass-door servosystem design is presented in reference 12.

Bypass-door steady-state gain. - The normal shock control systems used the overboard bypass-door area as the manipulated variable. Since the bypass-door exits were choked, the controller essentially manipulated the overboard bypass airflow. In the notation of figure 4, the transfer function representing the relation between the control-door bypass airflow and the command voltage to the bypass control-door servos is $K_b G_b$.

The value of the gain coefficient K_b is

$$K_b = 0.69 \frac{\text{kg/sec}}{\text{V}} \quad \text{long pipe}$$

$$K_b = 0.84 \frac{\text{kg/sec}}{\text{V}} \quad \text{choked orifice plate}$$

$$K_b = 1.04 \frac{\text{kg/sec}}{\text{V}} \quad \text{engine}$$

These gains are for three of the bypass doors driven from a common command voltage.

If wind-tunnel conditions and the inlet configuration had been the same for all tests, the value of K_b would have been the same regardless of the termination. However, for these tests K_b did have a different value for each inlet termination. Some changes

7

made during the program that caused changes in the value of K_b were (1) a change in bypass-door travel to feedback voltage gain after the long pipe tests to give a more convenient calibration during the choked orifice plate and engine tests; (2) the change in bleed configurations from II during the long pipe and choked orifice plate tests to I during the engine tests; and (3) the change in K_b with bypass-door operating point coupled with slightly varying operating points and magnitude of the airflow disturbance for the three different terminations.

Bypass-door dynamics. - The normalized frequency response of bypass-door position to command voltage is displayed in figure 13 and represents G_b. The figure indicates that the bypass-door response was flat within 0 to -3 decibels over the frequency range from 0 to 110 hertz. The 180° phase shift occurred at 120 hertz. Thus, since the dominant inlet resonance is at 55 hertz, the bypass doors would not be the limiting factor in trying to reduce the inlet resonance at 55 hertz.

TEST PROCEDURE

Test Setup

Figure 14 is a schematic representation of the inlet controls experiment as installed in the 10- by 10-Foot Supersonic Wind Tunnel. A small, 10-volt general purpose analog computer located in the control room was used to mechanize the controllers. The normal shock controls used P_{56} and/or P_{92} as feedback signals to manipulate the inlet bypass doors to control the normal shock. Three symmetrically spaced bypass doors were used for control; the other three bypass doors were used to generate a downstream airflow disturbance. Sinusoidal bypass-door airflow disturbances were generated over a frequency range from 0 to 140 hertz.

Operating Point Conditions

Typical inlet operating point conditions and disturbance magnitudes are given in table II.

The values of the gain coefficients presented in the previous sections were obtained by the technique of taking steady-state readings at the operating point and at the two extreme points of the sinusoidal disturbance before starting a frequency-response test. Thus, they represent the steady-state change in signal per change in disturbance. These gains were established at the normal operating point with the shock located near the center of the eight throat static-pressure taps (fig. 9). The zero-to-peak amplitude of shock excursion from the operating point was approximately 2.7 centimeters for the long pipe

TABLE II. - TYPICAL OPERATING POINT CONDITIONS

[Model angle of attack, zero.]

Free-stream Mach number, M_0	Reynolds number, Re^a	Ratio of specific heats, λ	Model configuration	Free-stream total pressure, H_0, N/cm^2	Free-stream temperature, T_0, K	Pressure ratio, H_e/H_0	Change in airflow (zero to peak), ΔW, kg sec	Change in normal shock displacement (zero to peak), ΔX, cm
2.5	3.88×10^6	1.40	Long pipe	8.93	318	0.92	0.22	2.7
2.5	3.88×10^6	1.40	Choked orifice plate	9.01	316	.92	.20	3.2
2.5	3.88×10^6	1.40	Engine	10.0	343	.92	.35	3.6
2.46^b	3.3×10^6	1.39	Long pipe	10.3	390	.93	.24	3.4

^{a}Based on the cowl lip diameter.

^{b}Conditions for running best control hot with long pipe configuration; results are shown in fig. 24.

termination, 3.2 centimeters for the choked orifice plate termination, and 3.6 centimeters for the engine termination.

Figure 15 indicates the gain characteristics of the shock position, P_{56}, and P_{92} as functions of the bypass door mass-flow ratio. The data were taken with the inlet terminated with the long pipe and a fixed choked plug position. The nominal operating point and excursion amplitude are noted in the figure.

When the normal shock is located near the throat (low values of bypass mass flow ratio), the shock is strongly influenced by the performance bleed (mass-flow ratios of about 0.01 to 0.03). The effect is to minimize shock motion and pressure variation in disturbed flow. In the normal operating range the bleed has small effect and the throat area against axial position is nearly constant (mass-flow ratios of about 0.04 to 0.08). Thus the shock position is more sensitive to flow variation than the pressures are. At the higher values of bypass mass-flow ratio (above about 0.12) the normal shock enters the diffuser, which has a high rate of change of area against axial position. This tends to reduce the shock-position sensitivity to flow variations. The pressures exhibited a higher sensitivity in this region since the normal shock is close to the pressure taps.

Steady-State and Dynamic Data

Both steady-state and dynamic data were taken. Steady-state data were taken by hand in the control room and also recorded in digital form on magnetic tape through the

use of the central automatic digital data encoder system (CADDE) for use at a later date.

The dynamic tests consisted of frequency response tests. For the dynamic tests both magnitude and phase data for a few key signals were determined on line using a commercial frequency response analyzer in the control room. These dynamic signals as well as others were recorded in analog form on magnetic tape for reduction at a later time. Before the dynamic tests, steady-state data were taken at the operating point and at each extreme point. These data gave the steady-state variations of the test signals. After correcting the dynamic data to account for dynamics of the disturbance device and the pressure transducers, the data were plotted in the form of Bode plots; these show magnitude and phase angle as a function of frequency. The open-loop and closed-loop magnitude data were normalized to the steady-state open-loop value.

ANALYSIS AND DESIGN MODEL

Figure 16 shows the inlet block diagram for disturbances originating downstream. At the top of the figure is a representation of the inlet showing the normal shock, the control signals, and the bypass doors. Also shown are the closed feedback loops from the inlet static pressures P_{56} and P_{92} which produce the command voltage V_b to the control bypass-door servos. The symbol $P_{56,com}$ represents the command value for the throat exit static pressure P_{56} by which the operator can set the position of the normal shock. The throat exit static pressure feedback controller transfer function is $K_{c56}G_{c56}$. The diffuser exit static pressure feedback controller transfer function is $K_{c92}G_{c92}$. When the inner P_{92} loop was used with the outer P_{56} loop, the P_{92} feedback signal was passed through a first-order high-pass filter before going to the P_{92} controller. The filter eliminates low-frequency signals in this loop, thereby preventing low-frequency interaction with the setting of the steady-state P_{56} pressure level and thus normal shock position. The filter transfer function is

$$\frac{1.67S}{1 + \dfrac{S}{0.6}}$$

The block diagram indicates the problem considered in this analysis, namely, to select control modes that will maintain desired P_{56} pressure levels and thus desired shock position at its command value while the inlet is subjected to a downstream airflow disturbance W_{bd}.

Before the experimental investigation of the normal shock control, various control systems were evaluated analytically using the root locus technique. Closed-loop system

10

performance was then verified with an analog computer simulation of the system.

To use the root locus technique, a transfer function representation was needed for both the bypass-door servos and the inlet dynamics.

Bypass-Door Servo Dynamic Model

To obtain the bypass-door transfer function, a mathematical model of the bypass-door servos was derived. This model was then modified to fit the experimental frequency response of bypass-door position to command voltage and was then simplified. The following transfer function was used to represent the bypass-door servos:

$$K_b G_b = \frac{K_b\left(\dfrac{S}{1010} + 1\right)}{\left(\dfrac{S}{650} + 1\right)\left[\dfrac{S^2}{1400^2} + 2(0.9)\dfrac{S}{1400} + 1\right]\left[\dfrac{S^2}{1500^2} + 2(0.2)\dfrac{S}{1500} + 1\right]}$$

where S is the Laplace operator.

With the appropriate value of K_b, this transfer function represents the control bypass-door airflow W_{bc} to command voltage V_b.

Inlet Dynamic Model

When the control system analysis was begun, experimental steady-state characteristics for the inlet had been established (ref. 9). The experimental dynamic data, as mentioned, were not then available, however. Based on the preceding steady-state inlet data, pressure signals with sufficient gain were chosen for feedback signals for the normal shock controllers.

Transfer functions for the inlet dynamics were obtained from an analog computer simulation. This simulation was based on linearized normal shock equations and one-dimensional wave equations for the subsonic duct. A description of this model and its simulation is found in reference 13.

The frequency responses of the selected control signals were determined from the analog simulation and then were curve fit to obtain the inlet transfer functions. The responses were obtained for downstream airflow disturbances. The simulated inlet was terminated with the long pipe and then with a choked orifice plate near the engine-face station. Since the long pipe produced more pronounced high-frequency resonances, the

controls analysis was concentrated on this case. It was considered to be the most difficult control problem.

Figure 17 shows normalized frequency response of shock position X to a downstream airflow disturbance W_{bd}. The short-dashed curve indicates results from the analog computer simulation, and the solid curve indicates the response of the simplified transfer function which was used to approximate the analog computer data. The transfer function approximation matches the analog computer data to 120 hertz. The long-dash line is the experimental open-loop response (ref. 8). It is included here for comparison purposes with the analytical models. The responses show that the reasonances occur at about the same frequencies. However, the experimental data show more attentuation and phase lag than the analytical model.

A similar process was applied to the other control signals, and it resulted in the transfer functions shown in table III. As indicated by the form of the transfer function $K_x G_x$, the relation between X and P_{56} is just a first-order lag with a corner at about 165 hertz. Since this is a fairly simple relation and since P_{56} is more directly measurable than X, P_{56} was used as the primary controller feedback signal instead of X. The throat exit static pressure P_{56} gives a fairly good indication of shock position X. It was also used as the signal to evaluate the performance of shock position control for

TABLE III. - FACTORED TRANSFER FUNCTIONS FOR INLET DYNAMICS

Ratio of variables	Factored transfer function	Block diagram symbols
$\dfrac{X}{W_{bd}}$	$\dfrac{K_{92}K_{56}K_x\left(\dfrac{S^2}{190^2}+\dfrac{0.84S}{190}+1\right)\left(\dfrac{S^2}{375^2}+\dfrac{0.94S}{375}+1\right)\left(\dfrac{S^2}{580^2}+\dfrac{0.28S}{580}+1\right)e^{-0.005S}}{\left(\dfrac{S}{46}+1\right)\left(\dfrac{S^2}{285^2}+\dfrac{0.30S}{285}+1\right)\left(\dfrac{S^2}{485^2}+\dfrac{0.34S}{485}+1\right)\left(\dfrac{S^2}{750^2}+\dfrac{0.34S}{750}+1\right)}$	$K_{92}G_{92}K_{56}G_{56}K_xG_x$
$\dfrac{P_{92}}{W_{bd}}$	$\dfrac{K_{92}\left(\dfrac{S}{1010}+1\right)\left(\dfrac{S^2}{190^2}+\dfrac{0.84S}{190}+1\right)\left(\dfrac{S^2}{375^2}+\dfrac{0.94S}{375}+1\right)\left(\dfrac{S^2}{580^2}+\dfrac{0.28S}{580}+1\right)}{\left(\dfrac{S}{46}+1\right)\left(\dfrac{S^2}{285^2}+\dfrac{0.30S}{285^2}+1\right)\left(\dfrac{S^2}{485^2}+\dfrac{0.34S}{485}+1\right)\left(\dfrac{S^2}{750^2}+\dfrac{0.34S}{750}+1\right)}$	$K_{92}G_{92}$
$\dfrac{P_{56}}{P_{92}}$	$K_{56}\,e^{-0.005S}$	$K_{56}G_{56}$
$\dfrac{X}{P_{56}}$	$\dfrac{K_x}{\dfrac{S}{1010}+1}$	K_xG_x

downstream airflow disturbances. It is recognized that, under flight conditions, P_{56} by itself would not suffice as a feedback variable. Corrections or biases might be required for changes in variables such as altitude, flight Mach number, and aircraft attitude. Also, for upstream disturbances that could cause choking of the inlet throat and thus an unstart, some sort of centerbody control would be required. These effects were not evaluated during this program.

The root locus analysis and design details for the various controllers are developed in appendix B. Appendix C presents the analytical and experimental data for controls tested other than the best control.

Types of Control Investigated

Both single-loop and two-loop control systems were investigated analytically and ex-

TABLE IV. - SUMMARY OF TYPES OF CONTROLLERS

INVESTIGATED

Type of control	General form of controller		P_{92} high-pass filter[a]
	P_{56} controller	P_{92} controller	
1	K	0	N[b]
2	$\dfrac{K\left(\dfrac{S}{a}+1\right)}{S}$	0	N
3	$\dfrac{K\left[\left(\dfrac{S}{\omega_n}\right)^2+\dfrac{2\rho}{\omega_n}S+1\right]}{S\left(\dfrac{S}{b}+1\right)}$	0	N
4	0	K'	Out
5	$\dfrac{K\left(\dfrac{S}{d}+1\right)}{S}$	K'	In
6	$\dfrac{K\left[\left(\dfrac{S}{\omega_n}\right)^2+\dfrac{2\rho}{\omega_n}S+1\right]}{S\left(\dfrac{S}{c}+1\right)}$	K'	In

[a]High-pass filter transfer function: $1.67S/(S/0.6+1)$.
[b]Not applicable.

perimentally. Six forms of controls were investigated. Table IV lists the general form of controls used and designates them types 1 to 6. For example, type 2 control is a single-loop proportional-plus-integral controller having P_{56} as its feedback signal. Type 5 control is a two-loop control using a proportional-plus-integral outer-loop controller that has P_{56} as its feedback signal and a proportional inner-loop controller that has P_{92} as its feedback signal. For the most part, just the control number will be used to describe the form of the controller being discussed. Many different pole-zero locations were investigated analytically for each of the type 2, 3, 5, and 6 controls. Only the controller giving the best response for each type of control is discussed in this report.

Controllers with integral action were investigated because they gave zero steady-state error in the face of step disturbances. Also, at low frequencies they gave good attenuation of the disturbance induced shock motion. The P_{92} inner loop with its associated high-pass filter was added in order to reduce the effects of the dead time between W_{bd} and P_{56}. The effectively decreased dead time results in less phase lag, which in turn makes the closed-loop system more stable. Thus, the P_{92} signal serves as an anticipatory signal for downstream airflow disturbances.

Control Evaluation

The control was used as a regulator to maintain a desired P_{56} (and thus shock position) while the inlet was perturbed by a downstream airflow disturbance. The throat exit static pressure P_{56} was used as the signal for evaluating performance. As represented by Bode plots, the ideal control would have an amplitude ratio of zero for all disturbance frequencies. Since this is not possible, the smaller the amplitude ratio the controlled system has, the better its performance. An additional requirement placed on the closed-loop response was that the closed-loop frequency response would not resonate above 1.3 times the open-loop steady-state value. With this amount of resonance, the normal shock still remained downstream of the geometric throat for all tests.

Controller Giving Best Response

Of the controllers investigated analytically, the one giving the best response was of the type 6 form (see table IV) two-loop compensated-integral system. This configuration turned out to be the best for the following reasons. The outer loop gave greater attenuation in shock motion (as indicated by P_{56}) over the frequency range from 0 to 7 hertz than did any of the other types of controls. This was accomplished while keeping the normalized closed-loop amplitude ratio resonance at 55 hertz below 1.3. The addition of the

14

filtered P_{92} inner loop resulted in the greatest attenuation of shock motion over the midfrequency range of 5 to 40 hertz.

RESULTS AND DISCUSSION

Summary of Analytical and Experimental Controls Investigated

Table V is a summary of various controllers used for both the analytical and experimental normal shock position controls investigation. It indicates the controllers used with the various inlet terminations and also the figures in which the data are presented. Only the control giving the best frequency response will be discussed in this section. The other controls that were used in the analytical and experimental investigations are discussed in appendixes B and C. The loop gain K_L will be explained in the next section.

Since the controls analysis was done only with the long pipe inlet termination, there will be no comparison of analytical and experimental data for the other inlet terminations. It might also be mentioned at this point that the closed-loop frequency response phase plots will not be included with most of the closed-loop data that are presented here and in the appendixes. However, for completeness the phase plots will be included with the data for the best control for each of the inlet terminations and with the data for unusual operating conditions.

Discussion of Best Control

Figure 18 compares the normalized closed-loop experimental and analytical $\Delta P_{56}/\Delta W_{bd}\big|_{CN}$ responses for the best control which is of the type 6 form for the inlet with the long pipe termination. The analytical curve was taken from figure 30 in appendix B. Both responses were taken at the same loop gain K_L. As indicated by equation (B10), at low frequencies, $P_{56}/W_{bd}\big|_{CN}$ is equal to ω/K_L. The value of K_L can be determined then by projecting the low-frequency part of the $P_{56}/W_{bd}\big|_{CN}$ curve (a straight line with a slope of +1) up until it crosses the magnitude ratio value of one. At this point $\omega = K_L$. Using this technique the loop gain K_L is 85 for the control used to get the responses shown in figure 18. The two responses compare fairly well except for the magnitude of the resonance at 60 hertz. The comparisons between the analytical and experimental responses for the type 1, 2, and 3 (see table IV) controls investigated are shown in figures 32, 35, and 37 in appendix C. They show a better agreement between the analytical and experimental responses than the two-loop best control did in figure 18.

15

TABLE V. - SUMMARY OF ANALYTICAL AND EXPERIMENTAL DATA

K_L	G_{c56}	G_{c92}	Variable plotted	Inlet termination	Used in figures
	Analytical data				
	Open loop	--	X	Long pipe	17
	Open loop	--	P_{56}		30,31
0.96	Proportional	0			30,32
79.	$(S/250 + 1)/S$	0			30,35
91.	$\dfrac{(S/285)^2 + (S/285) + 1}{S(S/500 + 1)}$	0			31,37
85.	$\dfrac{(S/325)^2 + (0.4S/325) + 1}{S(S/316 + 1)}$	2.50			18,31
	Experimental data				
	Open loop	--	X	Long pipe	5,17
	Open loop	--	P_{56}		6,19,33,34,38
	Open loop	--	P_{92}		7
0.67	Proportional	0	P_{56}		32,33
36.	$(S/250 + 1)/S$	0			36
79.	$(S/250 + 1)/S$	0			34,35,36,39
163.	$(S/250 + 1)/S$	0			36
104.	$\dfrac{(S/285)^2 + (S/285) + 1}{S(S/500 + 1)}$	0			37,38
0.32	0	Proportional	P_{92}		26
0.92	0	Proportional	P_{92}		26
1.6	0	Proportional	P_{92}		26
60.	$(S/250 + 1)/S$	0.5	P_{56}		39
60.	$(S/250 + 1)/S$	1.0			39
85.	$\dfrac{(S/318)^2 + (0.4S/318) + 1}{S(S/316 + 1)}$	0			27
85.	$\dfrac{(S/318)^2 + (0.4S/318) + 1}{S(S/316 + 1)}$	2.47			18,19,22,25,27

TABLE V. - Concluded. SUMMARY OF ANALYTICAL AND EXPERIMENTAL DATA

K_L	G_{c56}	G_{c92}	Variable plotted	Inlet termination	Used in figures
	Open loop	--	X	Choked orifice	5
	Open loop	--	P_{56}		6, 20, 41
	Open loop	--	P_{92}		7
63.	$(S/628 + 1)/S$	0	P_{56}		40
79.	$(S/628 + 1)/S$	1.0			40, 41
151.	$\dfrac{(S/318)^2 + (0.4S/318) + 1}{S(S/316 + 1)}$	1.10			42
79.	$\dfrac{(S/318)^2 + (0.4S/318) + 1}{S(S/316 + 1)}$	2.47			20, 22, 42
57.	$\dfrac{(S/318)^2 + (0.4S/318) + 1}{S(S/316 + 1)}$	2.75			23
75.	$\dfrac{(S/318)^2 + (0.4S/318) + 1}{S(S/316 + 1)}$	2.75			23
113.	$\dfrac{(S/318)^2 + (0.4S/318) + 1}{S(S/316 + 1)}$	2.75			23
	Open loop	--	X	Engine	5
	Open loop	--	P_{56}		6, 21, 44
	Open loop	--	P_{92}		7
88.	$(S/628 + 1)/S$	0	P_{56}		43
88.	$(S/628 + 1)/S$	3.0			43, 44
50.	$\dfrac{(S/318)^2 + (0.4S/318) + 1}{S(S/316 + 1)}$	0			45
35.	$\dfrac{(S/318)^2 + (0.4S/318) + 1}{S(S/316 + 1)}$	3.0			45
59.	$\dfrac{(S/318)^2 + (0.4S/318) + 1}{S(S/316 + 1)}$	3.0			21, 22, 45

Figure 19 shows a comparison of the normalized response of $\Delta P_{56}/\Delta W_{bd}$ for the experimental open-loop and closed-loop best control for the inlet terminated with the long pipe. The disturbance induced shock motion, as indicated by P_{56}, is reduced below that of the open-loop system over the frequency range from 0 to 50 hertz. At 1 hertz the P_{56} curve and, hence, shock motion are reduced to 7 percent of its open-loop value. Because of the integral control, there is zero steady-state error for step changes in downstream airflow disturbances. As shown in figure 19(b) the closed-loop phase angle starts from a 90° lead at low frequencies. This is the result of the P_{56} controller integral action being in the feedback path (the regulator problem). An integrator in the feedback path

looks like a differentiator in the closed loop and hence the closed-loop system starts at a 90° lead for low frequencies.

Figure 20 shows the response of P_{56} for the inlet terminated with the choked orifice plate using the control which produced the best results for the inlet terminated with the long pipe. It is noted in figure 20(a) that the closed-loop response of P_{56} is reduced below that of the open-loop response over the range in frequency from 0 to 40 hertz. At 1 hertz the amplitude of this signal has been reduced to 8 percent of its open-loop value.

Figure 21 shows the open- and closed-loop responses of P_{56} for the inlet terminated by the engine using the best control. The closed-loop amplitude ratio of P_{56} is below that of the open-loop over the frequency range from 0 to 50 hertz. At 1 hertz the disturbance induced shock motion is reduced to 11 percent of its open-loop value.

The normalized P_{56} amplitude responses of figures 19 to 21 have been replotted in figure 22. The curves show the controlled inlet's response with the long pipe, the choked orifice plate, and the engine terminations. It should be noted that the loop gain K_L was somewhat different in the three cases. From the similarity of these curves, it can be concluded that, under closed-loop control, the type of inlet termination has little effect on shock position response to a downstream airflow disturbance. This is desirable since the pneumatic impedance of a jet engine might change as its operating point changes.

Figure 23 shows a comparison of results obtained with the best control where the operating point and amplitude of shock motion is varied. Disregarding the differences in zero-to-peak amplitude between the curves, it is seen that the operating point for the solid curve is 2.5 centimeters forward of the normal operating point. Its higher valued low-frequency amplitude response implies that its loop gain is lower than that of the short-dash curve. The long-dash curve on the other hand has an operating point that is 1.2 centimeters downstream of the normal operating point. Its low-frequency amplitude response has lower values, implying that its loop gain is higher than that of the dashed curve. There are two factors that account for the differences in loop gain for the three responses. The first and most significant factor is the result of operating in the non-linear region of control bypass-door area to position curve as shown in figure 24. Moving the shock position to the forward operating point results in a lower control bypass-door area to position gain resulting in a lower K_b value thus decreasing the loop gain. Moving the shock position to the aft operating point results in a higher control bypass-door area to position gain resulting in a higher K_b value thus increasing the loop gain. The second and not quite as significant factor for the loop gain difference shown in figure 23 can be seen with the aid of figure 15 looking at the P_{56} against bypass mass-flow ratio curve. It is seen that the steady-state pressure gain $\Delta P_{56}/\Delta W_{bc}$ decreases or increases if the shock position operating point is moved forward or aft, respectively, of the normal operating point. These two factors combined to increase the loop gain when the shock position operating point was moved downstream and decreased when the shock

position operating point was moved upstream (see fig. 23). It is noted that the change in loop gain also affects high-frequency closed-loop performance; the magnitude of the resonance for the broken curve (highest loop gain) is significantly higher than those for the more forward shock operating points.

Figure 25 is a comparison of the normalized amplitude and phase shift for the best control run at two different free-stream total temperatures. The inlet was terminated with the long pipe. The free-stream total temperatures were 318 and 390 K. The other operating point conditions are shown in table II. The curves show that there is little variation in amplitude and phase shift as the free-stream total temperature was increased. The same control with the inlet terminated with the choked orifice plate was also run at tunnel free-stream total temperatures of 318 and 390 K. In this case (not shown) there was less difference between the hot and cold responses than there was when the inlet was terminated with the long pipe.

Figure 26 shows the experimental response of a proportional loop feeding back only P_{92} (type 4 control, which uses an unfiltered P_{92} as feedback). In this case only the inner loop of the block diagram of figure 16 is closed. The system was operated with three values of loop gain. Although the loop gain was varied by nearly five to one, the magnitude of the resonance at about 65 hertz did not vary significantly. The reason for this that the P_{92}/W_{bd} transfer function does not have as much dead time associated with it as the P_{56}/W_{bd} transfer function does. The lower dead time results in less phase lag which in turn makes the closed-loop system more stable.

The effect of this inner loop P_{92} feedback signal is demonstrated in figure 27 which shows the normalized magnitude plot of the best control while varying the inner loop (P_{92}) gain. By feeding back the diffuser exit signal, the disturbance induced shock motion (as indicated by P_{56}) can be significantly reduced in the range of about 4 to 30 hertz. This is done without significantly exciting the resonance at about 55 hertz. This result is in agreement with the results of the mathematical analysis.

SUMMARY OF RESULTS

Normal shock position controls were investigated for a Mach 2.5 axisymmetric mixed-compression inlet subjected to downstream airflow disturbances. Because of the fast bypass-door system, inherent inlet dynamics were the limitation on shock position control. Since the inherent inlet resonance was amplified for all the types of controls investigated, indications are that the fast bypass doors did not help in the resonance region. Comparison of the experimental and analytical results were good, thus verifying the simulation.

The best control of the inlet was accomplished with a two-loop control system feeding

back a throat exit static pressure and a diffuser exit static pressure. A proportional gain was used in the inner diffuser exit static pressure loop, and a compensated integral control was used in the outer throat exit static pressure loop. The diffuser exit static pressure signal went through a high-pass filter before going through its proportional controller.

The best control demonstrated the following:

1. The disturbance induced throat exit static pressure oscillations and hence normal shock position motion was reduced relative to its open-loop value over the frequency range from 0 to 40 hertz.

2. At 1 hertz the disturbance induced throat exit static pressure variations (hence normal shock position motion) were reduced to approximately 10 percent of the open-loop value; at lower frequencies the pressure variations and shock position excursion were further reduced in direct proportion to the frequency.

3. The use of the loop feeding back diffuser exit static pressure helped to reduce the effect of the dead time that existed between the diffuser exit airflow disturbance and the throat exit static pressure. The result was greater attenuation of shock position excursions (as implied by P_{56} responses) in the frequency range from 10 to 40 hertz.

4. Under closed-loop control the response of the inlet P_{56} pressure to downstream airflow disturbances was essentially independent of the type of termination: long pipe, choked orifice plate, or turbojet engine. This is desirable since the pneumatic impedance of a turbojet engine can vary with its operating point.

5. A significant change in closed-loop inlet response was produced by changing the normal shock position operating point. The different responses were the result of changes in the effective loop gain when going from one operating point to another. This resulted because of two factors. The first factor, of greater significance, resulted from operating the bypass doors in a nonlinear region of the area-to-position curve. A second factor resulted from operating the normal shock in regions of different effective bleed; this changed the pressure-to-flow gain.

6. The closed-loop response of the inlet was also unaffected by a change of 70 K in free-stream total temperature.

Lewis Research Center,
    National Aeronautics and Space Administration,
        Cleveland, Ohio, March 19, 1971,
            720-03.

APPENDIX A

SYMBOLS

A	area
$A, B, \ldots, H$	symbols representing eight throat static pressure taps
a, b, c, d	constants, 1/sec
BPD	bypass-door position
G	frequency dependent portion of transfer function
H	total pressure, N/cm^2
h	general feedback path transfer function
K, K'	gain factors
M	Mach number
m	mass flow, kg/sec
P_{56}	throat exit static pressure located at model station 56.1, N/cm^2
P_{92}	diffuser exit static pressure located at model station 92.2, N/cm^2
Re	Reynolds number based on cowl-lip diameter
S	Laplace operator, 1/sec
T	temperature, K
V	voltage, V
W	airflow, kg/sec
X	normal shock displacement, cm
α	model angle of attack, deg
γ	ratio of specific heats
Δ	indicates incremental change in variable
ρ	damping ratio
ω	frequency, rad/sec
ω_n	undamped natural frequency, rad/sec

Subscripts:

b	bypass door
c	control
com	command
c56	refers to controller transfer function that uses P_{56} as its feedback signal
c92	refers to controller transfer function that uses P_{92} as its feedback signal
d	disturbance
e	engine
L	loop
x	normal shock position
0	free stream
56	refers to transfer function relating P_{56} to P_{92}
92	refers to transfer function relating P_{92} to the diffuser exit airflow disturbance
$\vert_C$	denotes closed-loop transfer functions
$\vert_{CN}$	denotes closed-loop normalized transfer function
$\vert_N$	denotes open-loop normalized transfer function

APPENDIX B

ROOT LOCUS ANALYSIS AND DESIGN

Open-Loop Bypass-Door and Inlet Model Transfer Functions

The root locus technique was used for the analysis and design of the normal shock control systems. This required that the mathematical model be in the form of transfer functions. Open-loop experimental frequency responses of the appropriate inlet signals did not exist when the control analysis was performed. An analog inlet simulation (ref. 13) based on linearized normal shock equations and one-dimensional wave equations for the subsonic duct were used. Frequency responses were taken using the simulation. These responses were approximated to provide the transfer functions needed for the root locus analysis. The responses resulting from the simulated inlet terminated with the long pipe were used in the root locus design because this was considered a more difficult case than the inlet terminated with the choked orifice plate.

A block diagram of the inlet for downstream airflow disturbances is presented in figure 16. The transfer function $K_b G_b$ is the transfer function of control bypass door airflow (W_{bc}) to bypass-door command volts (V_b):

$$G_b = \frac{\left(\dfrac{S}{1010} + 1\right)}{\left(\dfrac{S}{650} + 1\right)\left[\dfrac{S^2}{1400^2} + \dfrac{2(0.9)S}{1400} + 1\right]\left[\dfrac{S^2}{1500^2} + \dfrac{2(0.2)S}{1500} + 1\right]} \tag{B1}$$

The transfer function $K_{92} G_{92}$ uses the transfer function relating diffuser exit static pressure (P_{92}) to bypass-door airflow (W_b):

$$G_{92} = \frac{\left[\dfrac{S^2}{190^2} + \dfrac{2(0.42)S}{190} + 1\right]\left[\dfrac{S^2}{375^2} + \dfrac{2(0.47)S}{375} + 1\right]\left[\dfrac{S^2}{580^2} + \dfrac{2(0.14)S}{580} + 1\right]\left(\dfrac{S}{1010} + 1\right)}{\left(\dfrac{S}{46} + 1\right)\left[\dfrac{S^2}{285^2} + \dfrac{2(0.15)S}{285} + 1\right]\left[\dfrac{S^2}{485^2} + \dfrac{2(0.17)S}{485} + 1\right]\left[\dfrac{S^2}{750^2} + \dfrac{2(0.17)S}{750} + 1\right]} \tag{B2}$$

and $K_{56} G_{56}$ is the transfer function relating throat exit static pressure (P_{56}) to P_{92}:

$$G_{56} = e^{-0.005S} \tag{B3}$$

A fourth order Pade approximation of the dead time was used in the inlet transfer function. The approximation is as follows:

$$e^{-0.005S} \approx \frac{\left[\dfrac{S^2}{1250^2} - \dfrac{2(0.965)S}{1250} + 1\right]\left[\dfrac{S^2}{1250^2} - \dfrac{2(0.655)S}{1250} + 1\right]}{\left[\dfrac{S^2}{1250^2} + \dfrac{2(0.965)S}{1250} + 1\right]\left[\dfrac{S^2}{1250^2} + \dfrac{2(0.655)S}{1250} + 1\right]} \tag{B4}$$

The transfer function $K_x G_x$ relates shock position X to P_{56}:

$$G_x = \frac{1}{\dfrac{S}{1010} + 1} \tag{B5}$$

The feedback transfer functions were assumed to be

$$h_{56} = h_{92} = 1.45 \text{ V/(N/cm}^2) \tag{B6}$$

Figure 28 illustrates the open-loop poles and zeros of the inlet and bypass-door transfer functions located in the S-plane. The poles are designated $\times$ and zeros are designated $\bigcirc$, as is conventional. The $\times$'s and $\bigcirc$'s enclosed in boxes represent the bypass-door dynamics G_b. The poles and zeros of the Padé network representing G_{56} are shown $\bigcirc$ and $\times$. The $\bigcirc$'s and $\times$'s represent the G_{92} dynamics.

Normal Shock Controller Design

A detailed root locus design will be discussed for only one type of controls: the type 2 single-loop controller feeding back the throat exit static pressure P_{56}. The controller is a proportional-plus-integral controller. Root locus design was also done for type 1, 3, 4, and 6 controls (see table IV for the general form of the various controls). The root locus design for these last four types of controls will not be shown.

As indicated by the form of the transfer function $K_x G_x$ (shock position X to throat exit static pressure P_{56}), the relation between shock position and P_{56} for a downstream airflow disturbance is just a first-order lag with a corner at about 165 hertz (see ref. 13 for calculations). Since this is a fairly simple relation and since P_{56} is more directly measurable than shock position, P_{56} was used as the primary feedback signal instead of

24

shock position. The throat exit static pressure P_{56} is the signal that will be used to evaluate the performance of the control to maintain a desired shock position while the inlet is subjected to a downstream airflow disturbance.

The control system using only P_{56} feedback is illustrated in figure 16 where the inner P_{92} loop is open. The command signal, $P_{56,com}$ is a voltage proportional to the desired throat exit static pressure. The controller $K_{c56}G_{c56}$ produces a command voltage, V_b which is supplied to the bypass-door servos.

Without control the transfer function relating P_{56} to the downstream airflow disturbance, W_{bd} is

$$\frac{P_{56}}{W_{bd}} = K_{92}K_{56}G_{92}G_{56}$$

With the single-loop P_{56} feedback control system, the response of P_{56} to the disturbance is

$$\left.\frac{P_{56}}{W_{bd}}\right|_C = \frac{K_{92}K_{56}G_{92}G_{56}}{1 + K_{c56}K_bK_{92}K_{56}G_{92}G_{56}G_{c56}G_bh_{56}} \tag{B7}$$

The problem is to specify the controller $K_{c56}G_{c56}$ that minimizes the disturbance induced P_{56} pressure fluctuations and, hence, shock motion, $\left.P_{56}/W_{bd}\right|_C$ over the frequency range of 0 to 140 hertz.

The transfer functions of the individual elements of the system are known in factored form. The root locus is used to determine the factors of the characteristic equation

$$1 + K_{c56}K_bK_{92}K_{56}G_{c56}G_bG_{92}G_{56}h_{56} = 0 \tag{B8}$$

In this case the controller transfer function $K_{c56}G_{c56}$ is of the general form (fig. 16)

$$\frac{K_{c56}\left(\frac{S}{c} + 1\right)}{S}$$

The integration provides infinite loop gain at zero frequency, thereby reducing the steady-state position error to zero for step disturbances.

Figure 29 shows the root locus plot for type 2 control. To the poles and zeros of the inlet and bypass doors of figure 28 are added a pole at the origin (the integrator) and a

zero at 250 radians per second (c = 250). These points are shown enclosed by a $\cup$ symbol in figure 29. A wide range of zero locations were investigated and the zero at 250 radians per second yielded the best performance.

The root locus plot indicates that the loci beginning at the integrator and inlet poles at 0 and 46 radians per second, respectively, terminate at the complex inlet zeros at 190 radians per second and 65°. The locus beginning at the open-loop bypass-door pole at 650 radians per second terminates at the controller zero at 250 radians per second. System stability is determined by the loci which originate at the inlet poles at 285 radians per second and 81° and cross the imaginary axes. The root locus indicates a maximum loop gain for stability to be 340.

Although the high-frequency loci determine stability gain, the low-frequency loci restrict the loop gain to less than 100 to maintain a reasonable damping ratio on the closed-loop poles in that region. A loop gain of 79 was chosen for the type 2 control.

The type 2 control along with three other types of controllers (types 1, 3, and 6) were then used on the analog simulation. Closed-loop frequency responses of $\Delta P_{56}/\Delta W_{bd}$ were obtained for each of the controllers. Many controllers of each type were investigated, but only the ones giving the best results for each type are presented. Figure 30 shows the responses for the open-loop, type 1 control, and type 2 control. Figure 31 shows the responses for the open-loop, control type 3 control, and type 6 control.

To assess the low-frequency performance of the single-loop integral type of controls, let us examine the low-frequency P_{56} pressure oscillations. The open-loop response of P_{56} to the disturbance becomes

$$\frac{P_{56}}{W_{bd}} = K_{92}G_{92}K_{56}G_{56}$$

Similarly, the closed-loop response becomes

$$\frac{P_{56}}{W_{bd}}\bigg|_C = \frac{K_{92}G_{92}K_{56}G_{56}}{1 + K_b G_b K_{c56} G_{c56} K_{92}G_{92}K_{56}G_{56}h_{56}}$$

A convenient normalization for the closed-loop response is

$$\frac{P_{56}}{W_{bd}}\bigg|_{CN} = \frac{\dfrac{P_{56}}{W_{bd}}\bigg|_C}{K_{92}K_{56}}$$

26

The normalized closed-loop response becomes

$$\frac{P_{56}}{W_{bd}}\bigg|_{CN} = \frac{G_{92}G_{56}}{1 + K_b G_b K_{c56} G_{c56} K_{92} G_{92} K_{56} G_{56} h_{56}} \tag{B9}$$

For small values of ω, equation (B9) reduces to (B10) remembering that G_{56}, G_{92}, G_x, and G_b equal one at low frequencies and that G_{c56} for the integral type of controls reduces to $1/\omega$ for small ω:

$$\frac{P_{56}}{W_{bd}}\bigg|_{CN} = \frac{1}{1 + \dfrac{K_L}{\omega}} \approx \frac{\omega}{K_L} \tag{B10}$$

where K_L is the loop gain.

The value of K_L can be obtained from the closed-loop frequency response. This can be done by projecting the low-frequency portion of the amplitude response line (a straight line with a slope of +1) until it crosses the amplitude ratio equals 1.0 line. At this point ω equals K_L.

Equation (B10) shows that at low frequencies, increasing K_L decreases the amplitude of the disturbance induced P_{56} pressure oscillations and hence normal shock motion. Although it would be desirable to have large values of loop gain, the control is limited by the instability generated by the loci crossing the imaginary axis. This discussion also applied to the two-loop type 6 control, only it is a little more complicated to show that equation (B10) also applies for small ω.

The loop gain for the type 1 control response shown in figure 30 was 0.96. The response of the type 2 control in figure 30 used a loop gain of 79. As expected, at low frequencies the response for this control shows a significant reduction of the disturbance induced P_{56} pressure oscillations. Because the controller is in the feedback path, the integrating action of the controller produces a closed-loop amplitude characteristic like that of a differentiator.

The controllers of the type 3 control were investigated next. Again the integrator was added to achieve good low-frequency control. Controllers with both distinct real zeros and complex quadratic zeros were investigated. The real pole was included to equate the order of the numerator and denominator, which gives finite high-frequency gain. This is necessary in a real system to avoid amplification of high-frequency noise. The best controller of this type was found to have the transfer function

$$K_{c56}G_{c56} \approx \frac{K_{c56}\left[\dfrac{S^2}{285^2} + \dfrac{2(0.5)S}{285} + 1\right]}{S\left(\dfrac{S}{500} + 1\right)} \tag{B11}$$

The dashed line of figure 31 is the analog computer response using the above controller. The loop gain was 91.

The control systems discussed were limited in performance by the dead time between the downstream airflow disturbance and the throat exit static pressure feedback signal P_{56}. In an attempt to obtain better regulation against downstream airflow disturbances, a control was investigated in which a diffuser exit static pressure P_{92} was used in addition to P_{56} for feedback. The transfer function $K_{92}G_{92}$ which relates P_{92} to the downstream airflow disturbance is modeled without the dead time. The pressure feedback P_{92} was used to augment the primary throat exit pressure loop. The P_{92} pressure has a rather low gain for use as the primary feedback signal. A simple proportional controller was chosen for the minor loop. Thus, $K_{c92}G_{c92}$ is replaced by K_{c92} in the block diagram of figure 16. The P_{92} pressure signal first went through a high-pass filter before going to the P_{92} proportional controller. The high-pass filter had the transfer function $1.67S/(S/0.6 + 1)$. Several compensated integral outer-loop controllers were investigated with the proportional inner loop. The best results were obtained with a controller having the transfer function:

$$K_{c56}G_{c56} \approx \frac{K_{c56}\left[\dfrac{S^2}{325^2} + \dfrac{2(0.15)S}{325} + 1\right]}{S\left(\dfrac{S}{316} + 1\right)} \tag{B12}$$

$$K_{c92} = 2.5 \tag{B13}$$

The long-dashed line of figure 31 is the analog computer response using the best type 6 control. The loop gain was 85. The long-dashed line response is below the short-dashed line response for frequencies above 4 hertz and demonstrates the advantage of using the P_{92} inner loop feedback.

28

APPENDIX C

ANALYTICAL AND EXPERIMENTAL DATA FOR CONTROLS TESTED

OTHER THAN THE BEST CONTROL

The data in this appendix are split up into three major groups. The first group is the data taken with the inlet terminated with the long pipe. The second and third groups are the data taken with the inlet terminated with the choked orifice plate and engine, respectively. The closed-loop frequency response phase plots will not be included with most of the closed-loop data that are presented in this appendix.

Inlet Terminated with Long Pipe

Single-loop and double-loop control systems were investigated on the long pipe configuration (type 1, 2, 3, and 5 controls).

Single-loop throat exit static pressure feedback (types 1, 2, and 3 controls). - Figure 16 shows that the single-loop control of shock position feeding back throat exit static pressure P_{56} is represented by setting $K_{c92}G_{c92} = 0$.

Type 1 controls: Figure 32 shows a comparison between the analytical frequency response and the experimental response for type 1 control. The analytical curve was taken from figure 30 in appendix B. The analytical response had a slightly higher loop gain than the experimental response did. The analytical response also shows a slightly increased resonance. Except for the loop-gain difference, the responses compare favorably from 0 to 80 hertz. There seems to be some discrepancy above 80 hertz; this is probably due to the simplification introduced in the analytical model at the higher frequencies.

Figure 33 shows the experimental frequency response of P_{56} to a downstream airflow disturbance using type 1 control compared with that of the open-loop response (solid line). The curves show that the distrubance induced shock motion has been reduced below that of the open-loop from 0 to 45 hertz. The curves also show that the resonance at about 55 hertz has been increased over that of the open-loop system. Adding closed-loop control has improved system response at frequencies below the resonance frequency, but it has not improved the system response in the area of the resonance and, in fact, has made it worse in that region. Also, because proportional control was used, a steady-state error in P_{56} will exist for steady-state changes in W_{bd}. For type 1 control (fig. 33) a step disturbance in airflow will produce an offset in P_{56} and thus shock position having a value 0.6 of that of the open-loop system. This error can be limited by using some

form of integral control for G_{c56}. All of the other controls discussed will be some form of integral control.

The amplitude of P_{56} and thus shock motion induced by the disturbance airflow when the system is under closed-loop control can be determined by the methods of classical control theory. With the aid of figure 16 the disturbance airflow W_{bd} can be considered to be the input to a closed-loop servomechanism having $K_{56}G_{56}K_{92}G_{92}$ as its forward path transfer function and $h_{56}K_{c56}G_{c56}K_bG_b$ in the feedback path. The K_xG_x block is outside of the closed-loop and in series with its output. The transfer function of the closed-loop would then, in general, be given by $G/(1 + Gh)$ where G and h, represent the forward path and feedback path transfer functions, respectively. Thus

$$\left.\frac{P_{56}}{W_{bd}}\right|_C = \frac{K_{56}K_{92}G_{56}G_{92}}{1 + K_{56}K_{92}h_{56}K_{c56}K_bG_{56}G_{92}G_{c56}G_b} \tag{C1}$$

The open-loop response of throat exit static pressure to the disturbance airflow would be given by

$$\frac{P_{56}}{W_{bd}} = K_{56}K_{92}G_{56}G_{92} \tag{C2}$$

At low frequencies $G_{56} = G_{92} \cong 1$, hence,

$$\frac{P_{56}}{W_{bd}} = K_{56}K_{92} \quad \text{for small } \omega \tag{C3}$$

This is a convenient normalizing parameter. The closed-loop normalized transfer function of P_{56} to W_{bd} is

$$\left.\frac{P_{56}}{W_{bd}}\right|_{CN} = \frac{\left.\dfrac{P_{56}}{W_{bd}}\right|_C}{K_{56}K_{92}} = \frac{G_{56}G_{92}}{1 + K_{56}K_{92}h_{56}K_{c56}K_bG_{56}G_{92}G_{c56}G_b} \tag{C4}$$

and for small values of ω

$$\left.\frac{P_{56}}{W_{bd}}\right|_{CN} = \frac{1}{1 + K_{56}K_{92}h_{56}K_{c56}K_b} = \frac{1}{1 + K_L} \tag{C5}$$

30

where K_L is the loop gain. It is thus seen that the low-frequency disturbance induced shock motion can then be reduced by increasing the loop gain. However, increasing the loop gain also has the disadvantage of increasing the resonance at 55 hertz.

Type 2 control: Next, single-loop proportional-plus-integral control feeding back only P_{56} was investigated. In this case

$$G_{c56} = \frac{\dfrac{S}{a} + 1}{S}$$

Equation (C4) reduces to equation (C6) when $G_{56} = G_{92} = G_b = 1$ at low frequencies. Thus,

$$\left.\frac{P_{56}}{W_{bd}}\right|_{CN} = \frac{1}{1 + \dfrac{K_L}{\omega}} \approx \frac{\omega}{K_L} \quad \text{for small } \omega \tag{C6}$$

where K_L is the loop gain. Therefore, in the low-frequency range the amplitude characteristic increases in direct proportion to the frequency like that of a differentiator. This is due to the fact that the integrator, whose output amplitude decreases with frequency, provides a progressively smaller feedback signal as frequency is increased. This effectively approaches opening the feedback loop resulting in no control. The resulting closed-loop response is displayed in figure 34. The transfer function used for the controller was

$$\frac{K_{c56}\left(\dfrac{S}{250} + 1\right)}{S}$$

The value of loop gain can be determined by projecting the slope of the low-frequency portion of the amplitude characterisic (a straight line with a slope of +1) to unity amplitude. From figure 34 it is seen that $K_L = 79$. Significant reduction in P_{56} and thus shock motion at the lower frequencies is noted with this type of control. At 1 hertz the disturbance induced P_{56} pressure oscillations and thus shock motion is approximately 8 percent of the corresponding open-loop value. The phase shift of the closed-loop system displays a 90° leading characteristic at low frequencies, which is indicative of a differentiator. The disturbance induced P_{56} pressure oscillations and thus shock motion is less than that of the open-loop out to 8 hertz. The resonance at 55 hertz has not been improved over that of the open-loop but the control has zero error in the steady-state.

Figure 35 shows a comparison of the type 2 control experimental and analytical data. The solid line represents the analytical data. The analytical curve was taken from figure 30 in appendix B. Analysis showed that the $K_{c56}(S/250 + 1)/(S)$ controller gave the best results for the type 2 control. It is the one used for both figures 34 and 35. Figure 35 shows that the loop gain was the same for both the analytical and experimental data. The experimental and analytical resonance frequency and magnitude agree well.

Figure 36 shows experimental data using the type 2 control and varying the controller gain, which in turn varies the loop gain. As shown in figure 36 the increasing loop gain results in a greater attenuation of low-frequency shock motion. However, at the same time the resonance amplitude at about 50 hertz is increased. The choice of the value of loop gain is then a trade-off between low- and high-frequency performance.

Type 3 control: Next a compensated integral control (type 3) was tested. Here the controller transfer function was of the form

$$K_{c56}G_{c56} = K_{c56} \frac{\left(\dfrac{S}{\omega_n}\right)^2 + \dfrac{2\rho}{\omega_n}S + 1}{S\left(\dfrac{S}{a} + 1\right)}$$

Figure 37 shows a comparison of the experimental and analytical responses for the type 3 control. The analytical curve was taken from figure 31 in appendix B. Figure 37 shows that the loop gain was almost the same for both the analytical and experimental data. The resonant frequencies and magnitudes agree well.

Figure 38 shows a comparison of the experimental open-loop response with that of the type 3 control. Again, because of the presence of an element with integral action in the feedback path, the closed-loop amplitude characteristic increases in direct proportion to the frequency. At 1 hertz the disturbance induced P_{56} pressure oscillations and thus shock motion is reduced to only 6 percent of its open-loop value. The amplitude of the P_{56} and thus shock motion is reduced below that of the open-loop response in the frequency range from 0 to 9 hertz. The closed-loop system displays a slight amplification of shock motion at the resonant frequency as compared with its open-loop value.

Two-loop control feeding back throat exit and diffuser exit static pressures (type 5 control). - Figure 16 shows the block diagram of the system feeding back both a throat exit static pressure P_{56} and a diffuser exit static pressure P_{92} using a filtered P_{92} signal. The addition of the inner loop thus enabled the normal shock position control to react faster to downstream airflow disturbances than is possible with only P_{56} feedback because the effective dead time between W_{bd} and P_{56} is reduced by using P_{92}, which has very little dead time between it and W_{bd}.

Figure 26 demonstrates P_{92}'s anticipatory action to downstream airflow disturbances. Figure 26 shows the experimental response of the type 4 control feeding back only an unfiltered P_{92} signal. In this case only the inner loop of the block diagram of figure 16 is closed. The system was operated with three values of loop gain. Figure 26 shows that, although the loop gain was varied by nearly five to one, the magnitude of the resonance at 65 hertz did not vary significantly. This decreased dead time results in less phase lag, which in turn makes the closed-loop system more stable as figure 26 shows.

Figure 39 shows the experimental normalized amplitude response curves using the type 5 control, while varying the proportional gain for the P_{56} and filtered P_{92} feedback loops.

The broken curve had an open inner loop while the loop gain of the proportional-plus-integral controller in its outer loop was slightly higher than that for the other two curves. The dashed curve had a proportional gain of 0.5 for the inner loop. The solid curve had an inner loop proportional gain of 1. It can be seen that feeding back P_{92} improves the response of the system in the midfrequency range (3 to 55 Hz) in the case where a porportional-plus-integral controller is used in the outer loop.

Inlet Terminated with Choked Orifice Plate

Type 5 control. - Figure 40 shows the experimental results for the best type 5 controller used with the inlet terminated with choked orifice plate. The solid curve represents the experimental response with no inner loop P_{92} feedback ($K_{c92}G_{c92} = 0$). The dashed curve represents the case where proportional filtered P_{92} feedback ($K_{c92}G_{c92} = 1.0$) was used. The data show that feeding back P_{92} improves the performance of the control in the midfrequency range with the inlet terminated with the choked orifice plate. In this instance it also appears to have slightly increased the effective loop gain of the system by lowering the 1 hertz amplitude ratio.

In figure 41 the normalized amplitude response of the type 5 control (fig. 40) is compared with that of the open-loop system. The amplitude of shock excursion deduced from P_{56} pressure for the closed-loop system is reduced over the frequency range from 0 to 34 hertz (fig. 41) as compared with the open-loop system. At 1 hertz the disturbance induced P_{56} pressure oscillations and hence shock motion has been reduced to 8 percent of its open-loop value.

Type 6 control. - Figure 42 shows the experimental normalized magnitude of the response of the type 6 control showing the effects of the inner- and outer-loop gain variation. The solid curve had a higher value of outer-loop gain (P_{56} feedback) and a lower value of inner-loop gain (filtered P_{92} feedback) than those values for the dashed curve.

33

The figure shows that the performance at lower frequencies (7 Hz and below) is improved by the higher value of outer-loop gain and that performance at the midfrequencies (7 to 40 Hz) is improved by higher inner-loop gain. Improved response to 40 hertz, is obtained by increasing the gains; but, as the gains are increased, the magnitude of the resonance at 55 hertz is also increased. Therefore, a compromise has to be reached in which good response below 40 hertz is traded off against an increase in the resonance at 55 hertz.

Inlet Terminated with Engine

Type 5 control. - Figure 43 shows the closed-loop experimental response of P_{56} where a proportional-plus-integral control is used for the outer loop and the inlet is terminated by the J85-13 engine operating at 80.6 percent corrected speed. In the case represented by the solid curve, no inner loop feedback of the filtered P_{92} signal was used. The inner loop was closed using $K_{c92}G_{c92} = 3.0$ in the case represented by the dashed curve. It is noted that closing the inner loop reduces shock position excursion as represented by P_{56} in the frequency range from 1 to 50 hertz.

Figure 44 shows a comparison of the experimental response of the open-loop system to that of the type 5 control. The disturbance induced shock motion as indicated by P_{56} is reduced to 7 percent of its open-loop value at 1 hertz. The response of the closed-loop system is improved from its open-loop value over the frequency range from 0 to 35 hertz while the magnitude of the resonance at 55 hertz has been increased.

Type 6 control. - In figure 45 the effect of changing outer-loop and inner-loop gains is presented for the type 6 control with the inlet terminated with the J85-13 turbojet engine. In the case of the dashed curve no inner-loop feedback (filtered P_{92}) was used. In the cases of the solid and broken curves the same value of inner-loop gain was used, but the outer-loop gain was greater in the case of the solid curve. It is noted that the low-frequency attenuation of shock motion as indicated by P_{56} is increased by use of a higher outer-loop gain.
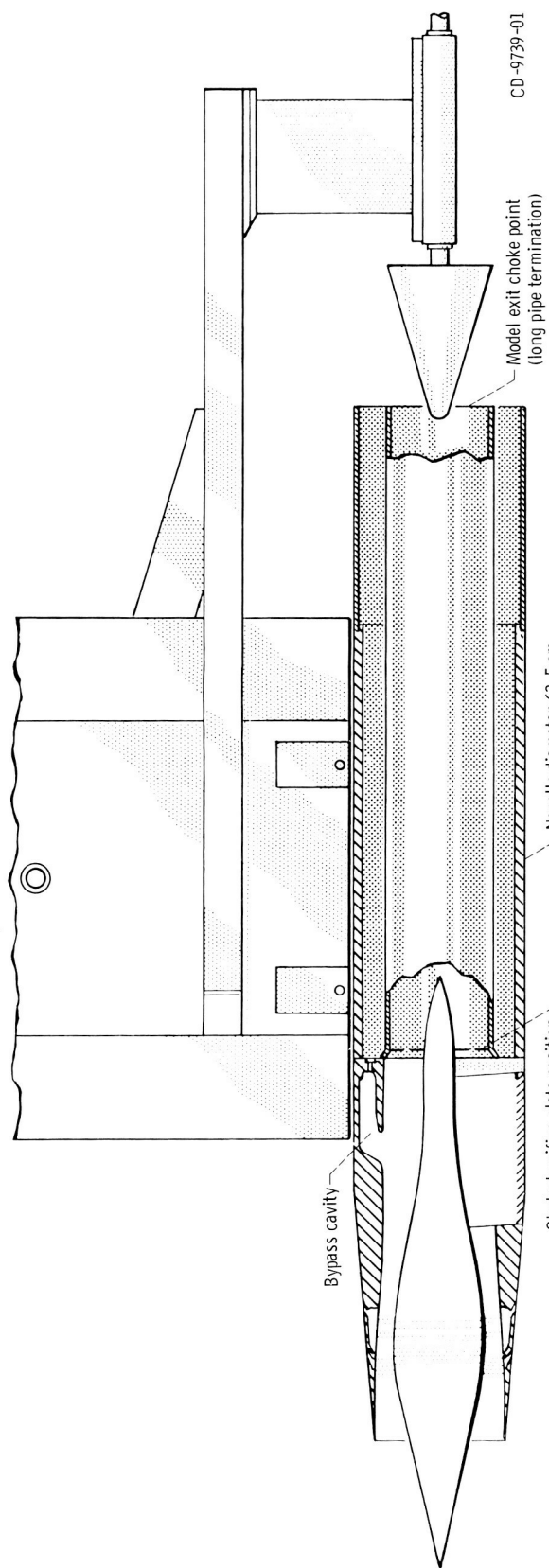
REFERENCES

1. Bowditch, David N.; and Wilcox, Fred A.: Dynamic Response of a Supersonic Diffuser to Bypass and Spike Oscillations. NASA TM X-10, 1959.

2. Anderson, Bernard H.; and Bowditch, David N.: Investigation of Inlet Control Parameters for an External-Internal Compression Inlet From Mach 2.1 to 3.0. NACA RM E58G08, 1958.

3. Chun, K. S.; and Burr, R. H.: A Control System Concept for an Axisymmetric Supersonic Inlet. J. Aircraft, vol. 6, no. 4, July-Aug. 1969, pp. 306-311.

4. Nettles, J. C.; and Leissler, L. A.: Investigation of Adjustable Supersonic Inlet in Combination With J34 Engine Up to Mach 2.0. NACA RM E54H11, 1954.

5. Leissler, L. Abbott; and Nettles, J. Cary: Investigation to Mach Number 2.0 of Shock-Positioning Control Systems for a Variable-Geometry Inlet in Combination with a J34 Turbojet Engine. NACA RM E54I27, 1954.

6. Wilcox, Fred A.: Investigation of a Continuous Normal-Shock Positioning Control for a Translating-Spike Supersonic Inlet in Combination With J34 Turbojet Engine. NACA RM E57G16, 1957.

7. Schweikhardt, R. G.; and Grippe, R. P.: Investigations in the Design and Development of a Bypass Door Control System for an SST Axisymmetric Intake Operating in the External Compression Mode. Paper 70-695, AIAA, June 1970.

8. Wasserbauer, Joseph F.: Dynamic Responses of a Mach 2.5 Axisymmetric Inlet with Engine or Cold Pipe and Utilizing 60 Percent Supersonic Internal Area Contraction. NASA TN D-5338, 1969.

9. Cubbison, Robert W.; Meleason, Edward T.; and Johnson, David F.: Performance Characteristics from Mach 2.58 to 1.98 of an Axisymmetric Mixed-Compression Inlet System with 60-Percent Internal Contraction. NASA TM X-1739, 1969.

10. Cubbison, Robert W.; Meleason, Edward T.; and Johnson, David F.: Effect of Porous Bleed in a High-Performance Axisymmetric, Mixed-Compression Inlet at Mach 2.50. NASA TM X-1692, 1968.

11. Zeller, John R.: Design and Analysis of a Modular Servoamplifier for Fast-Response Electrohydraulic Control Systems. NASA TN D-4898, 1968.

12. Neiner, George H.: Servosystem Design of a High-Response Slotted-Plate Overboard Bypass Valve for a Supersonic Inlet. NASA TN D-6081, 1970.

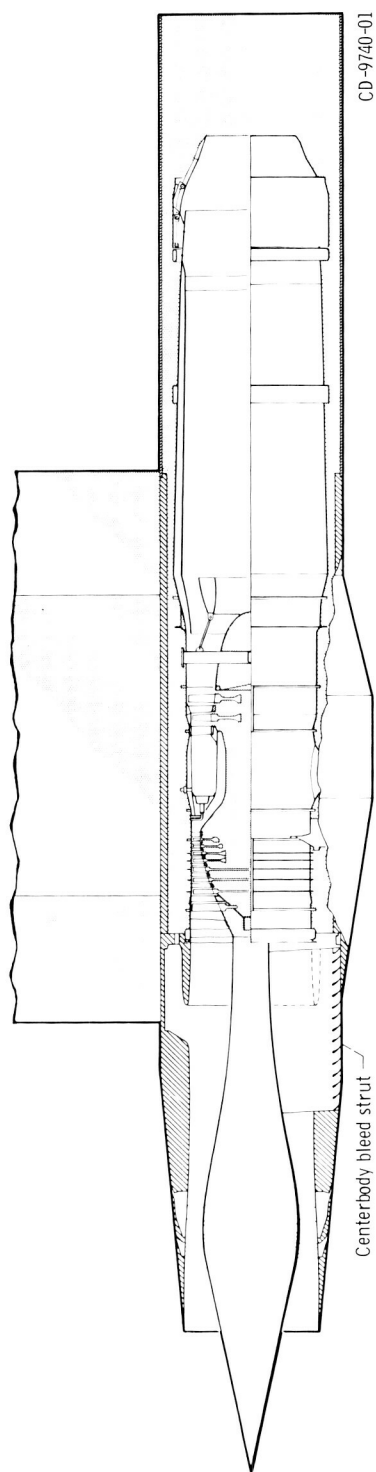13. Willoh, Ross G.: A Mathematical Analysis of Supersonic Inlet Dynamics. NASA TN D-4969, 1968.
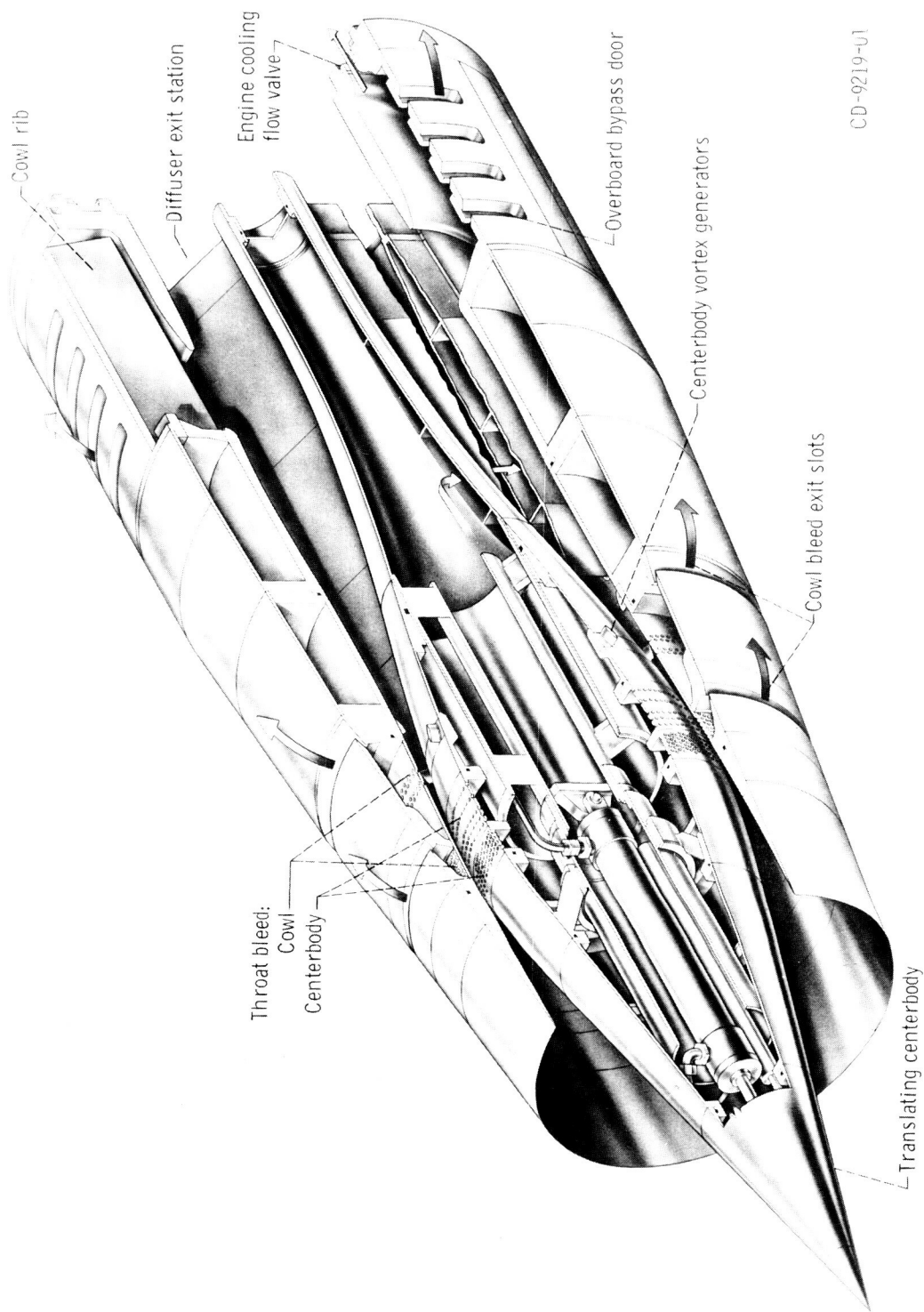
Figure 1. – Isometric view of inlet model.

Cowl rib

Diffuser exit station

Engine cooling flow valve

Overboard bypass door

Centerbody vortex generators

Cowl bleed exit slots

Throat bleed:
Cowl
Centerbody

Translating centerbody

CD-9219-U1

36

CD-9739-01

Model exit choke point
(long pipe termination)

Nacelle diameter 63.5 cm

Choked orifice plate position

Bypass cavity

(a) Inlet-long pipe and choked orifice configuration.

CD-9740-01

Centerbody bleed strut

(b) Inlet-engine configuration.

Figure 2. - Inlet terminations.

37
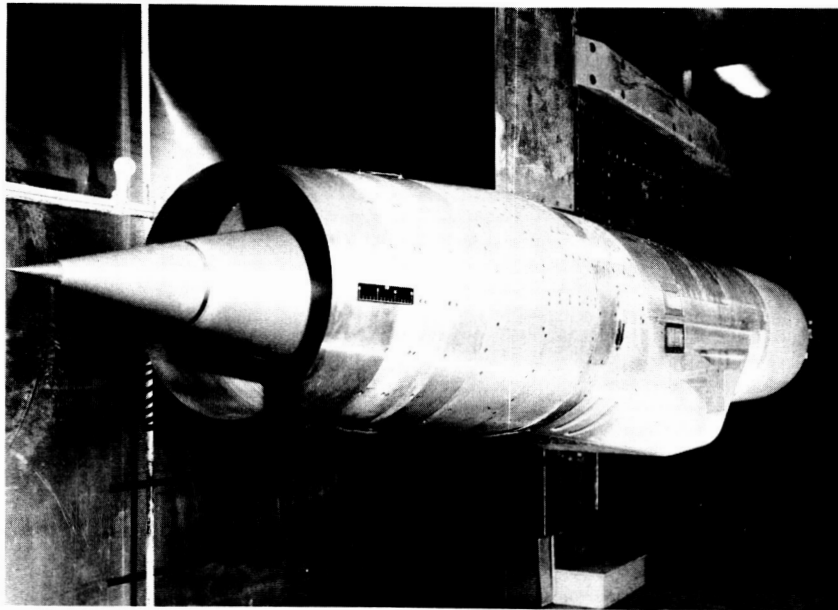
C-68-943

Figure 3. – Model installed in 10- by 10-foot Supersonic Wind Tunnel test section.

$$\frac{P_{92}}{W_{bd}} = K_{92}G_{92}$$

$$\frac{P_{56}}{W_{bd}} = K_{92}G_{92}K_{56}G_{56}$$

$$\frac{X}{W_{bd}} = K_{92}G_{92}K_{56}G_{56}K_xG_x$$
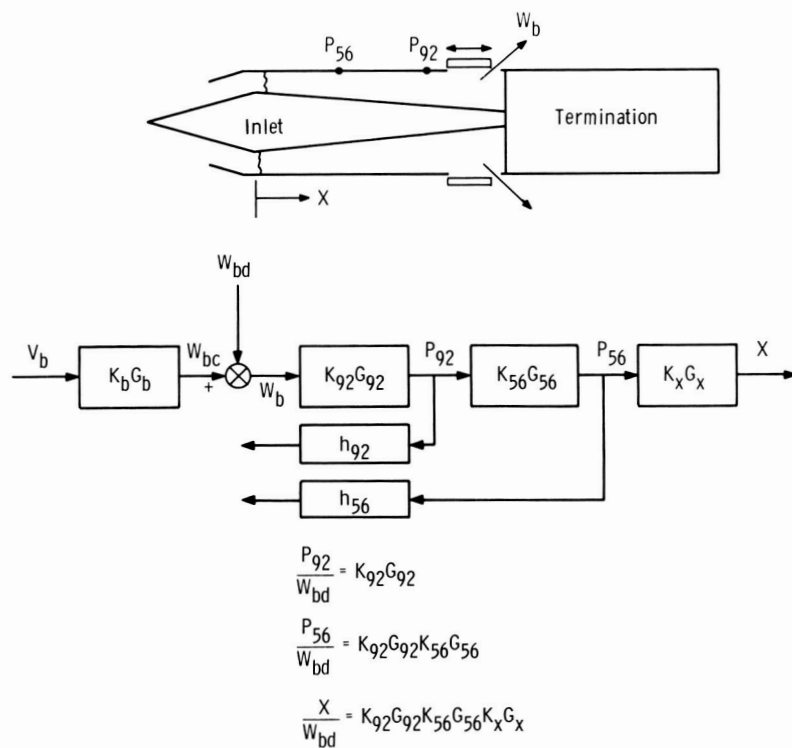
Figure 4. – Block diagram of inlet.
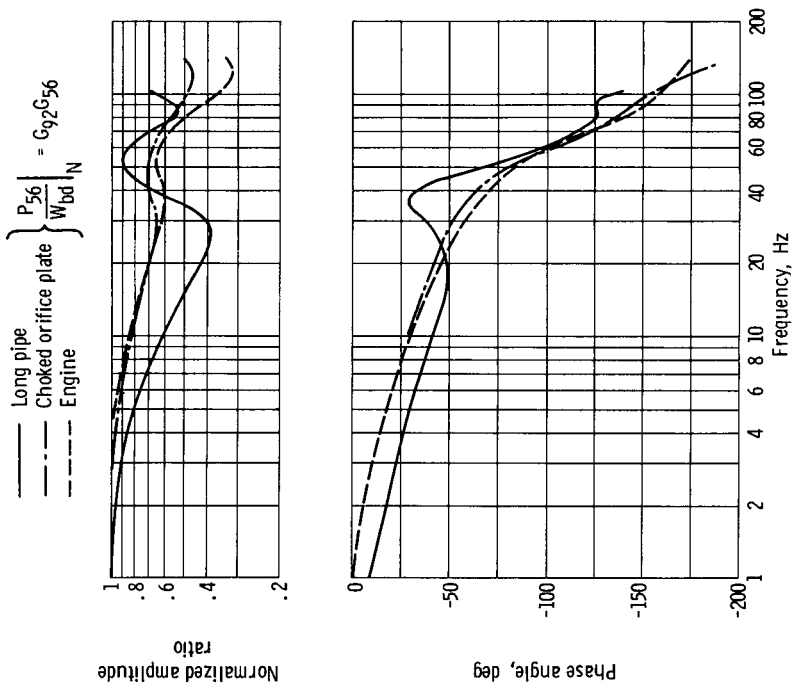
Figure 6. - Frequency response of throat exit static pressure P_{56} to downstream airflow disturbances for different inlet terminations (data from ref. 8).

$$\left.\begin{array}{c}\text{Long pipe}\\\text{Choked orifice plate}\\\text{Engine}\end{array}\right\}\quad \frac{P_{56}}{W_{bd}}\Big|_N = G_{92}G_{56}$$

Frequency, Hz

Normalized amplitude ratio

Phase angle, deg
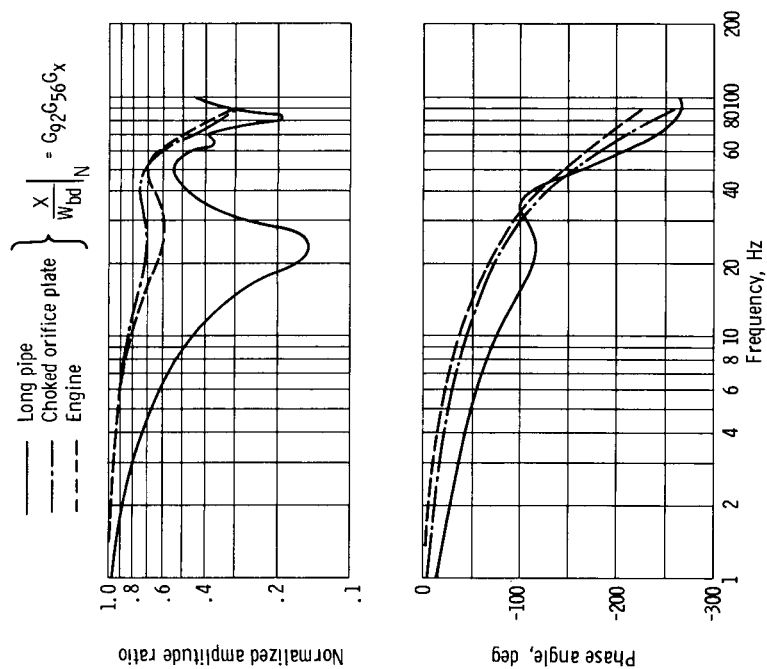
Figure 5. - Frequency response of normal shock position to downstream airflow disturbances for different inlet terminations (data from ref. 8).

$$\left.\begin{array}{c}\text{Long pipe}\\\text{Choked orifice plate}\\\text{Engine}\end{array}\right\}\quad \frac{X}{W_{bd}}\Big|_N = G_{92}G_{56}G_X$$

Frequency, Hz

Normalized amplitude ratio

Phase angle, deg

39
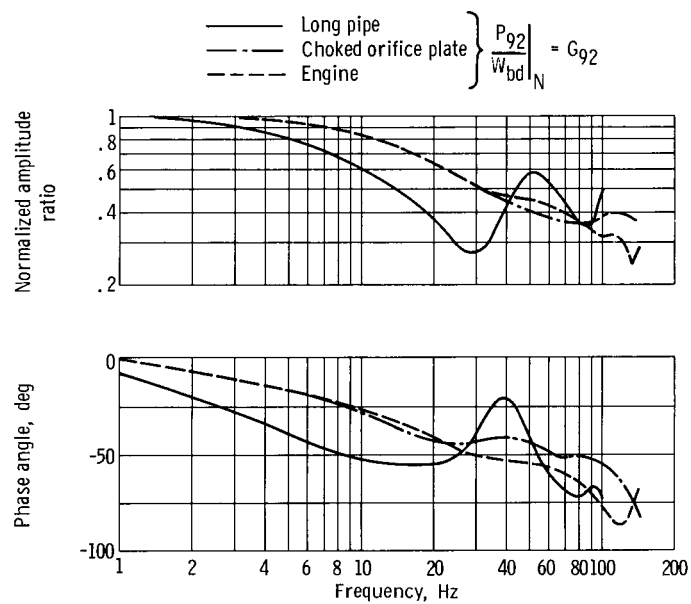
Figure 7. – Frequency responses of diffuser exit static pressure P_{92} to downstream airflow disturbances for different inlet terminations (data from ref. 8).
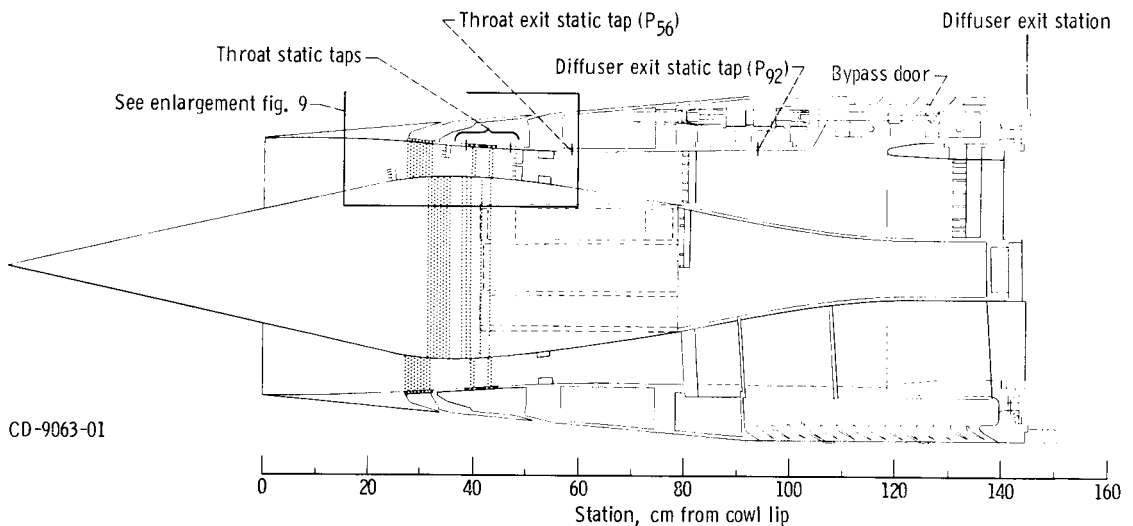
Figure 8. – Location of pressure instrumentation.

CD-9063-01
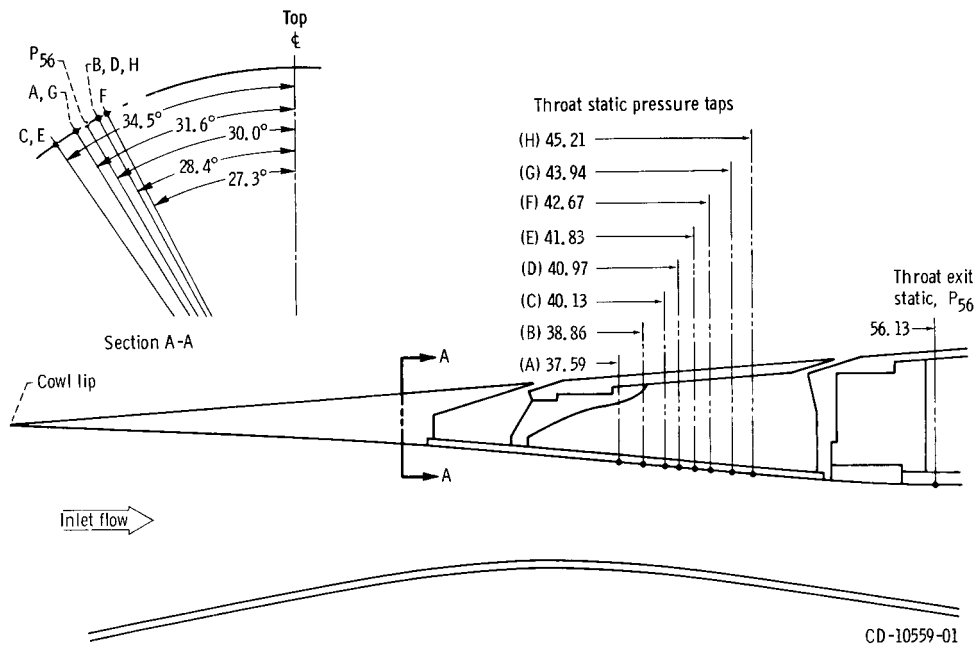
Figure 9. - Inlet throat pressure instrumentation locations. (Dimensions in centimeters from cowl-lip.)

(a) Amplitude ratio.

(b) Phase angle.
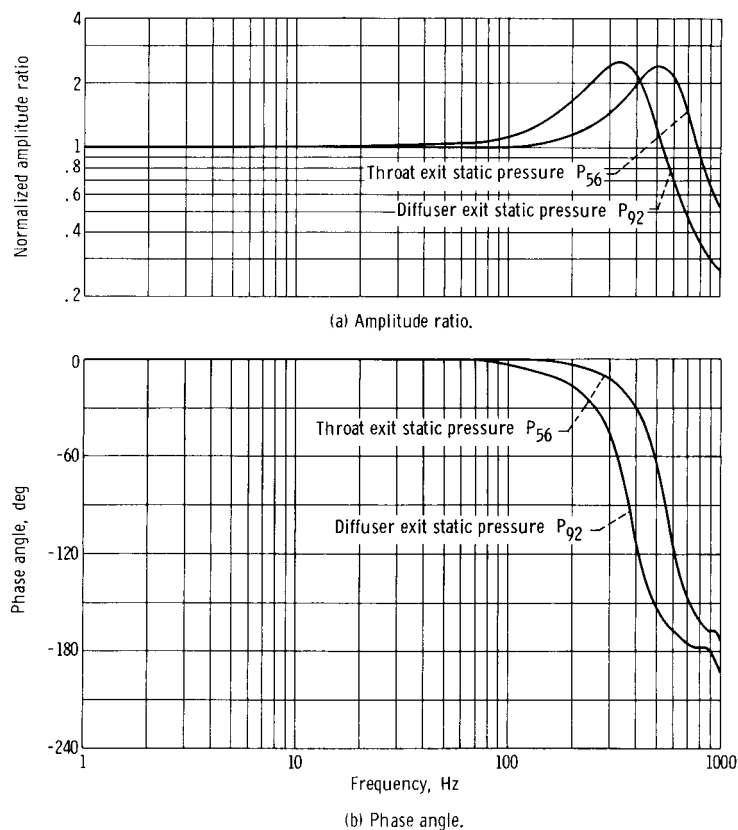
Figure 10. - Frequency response plots of feedback pressure transducers and connecting tubing.

41

Hydraulic actuator

Position sensor

CD-9062-01
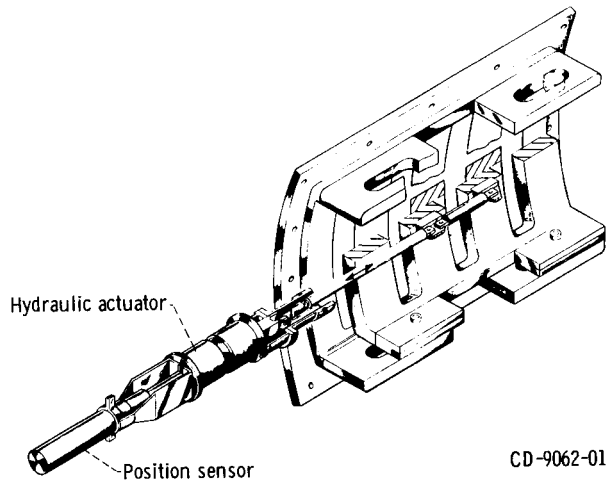
Figure 11. - Overboard bypass door assembly and actuator.

Command

Servo-
amplifier

Free stream ➡

Nacelle wall

Servovalve

Actuator

Bypass airflow

Feedback
transducer
servovalve

Inlet airflow ➡
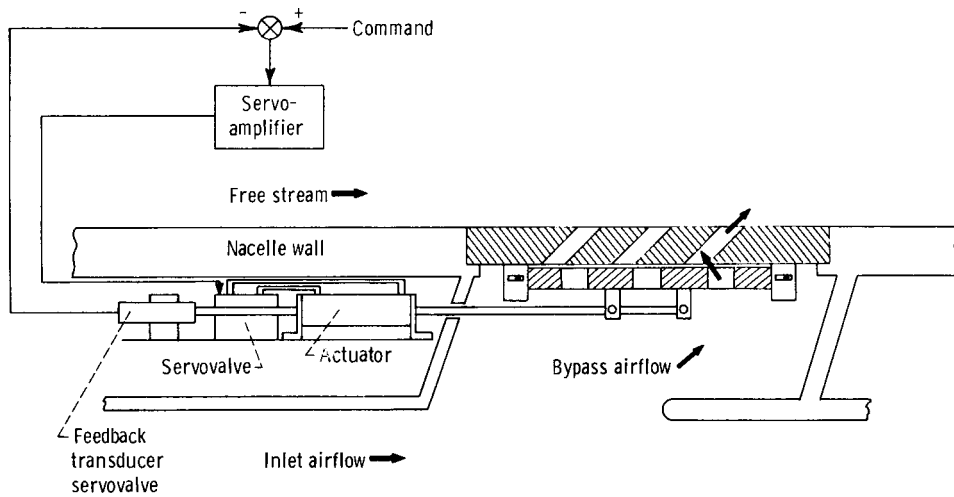
Figure 12. - Bypass-door servosystem installation.
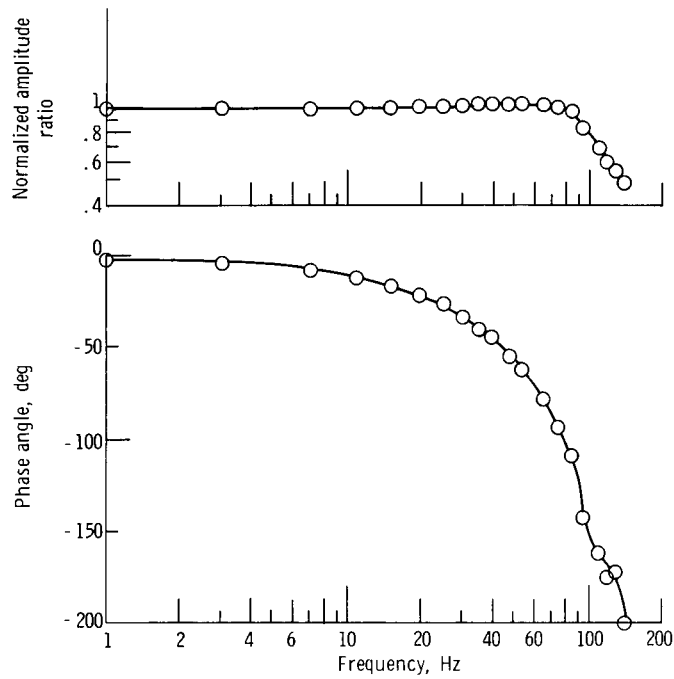
Figure 13. - Normalized bypass-door position to command voltage
frequency response.
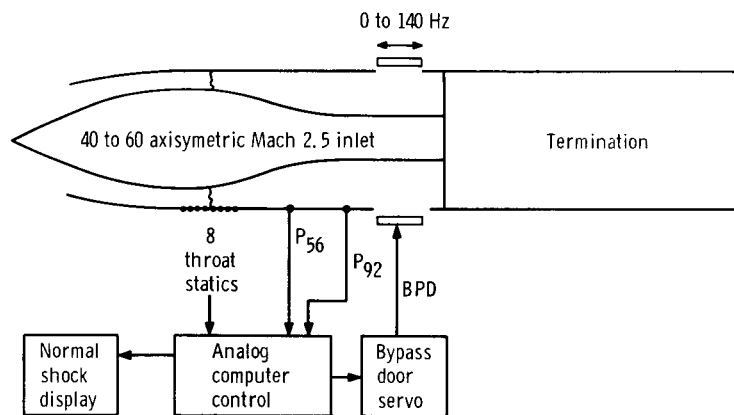
Figure 14. - Schematic representation of inlet controls experiment in 10- by 10-foot
Supersonic Wind Tunnel.
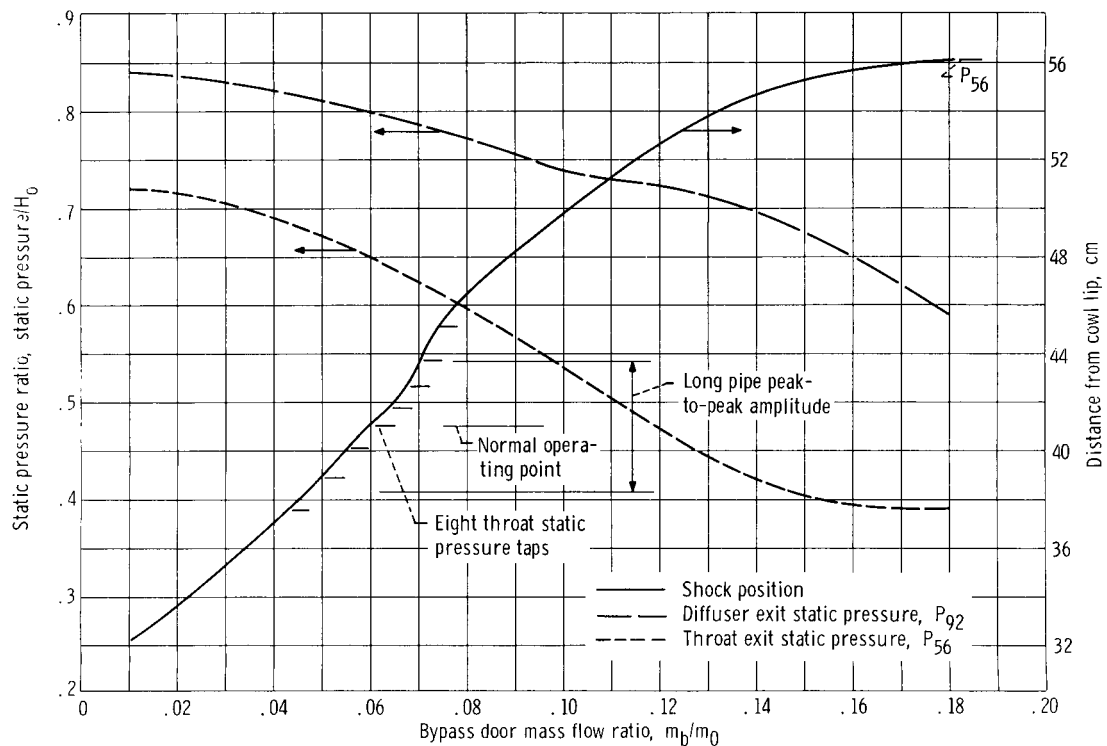
Figure 15. - Shock position, P_{56}, and P_{92} gain characteristics as function of bypass-door mass-flow ratio with inlet terminated by long pipe. Free-stream total pressure, 10.6 N/cm^2; free-stream mass flow m_0, 16.2 kg/sec.
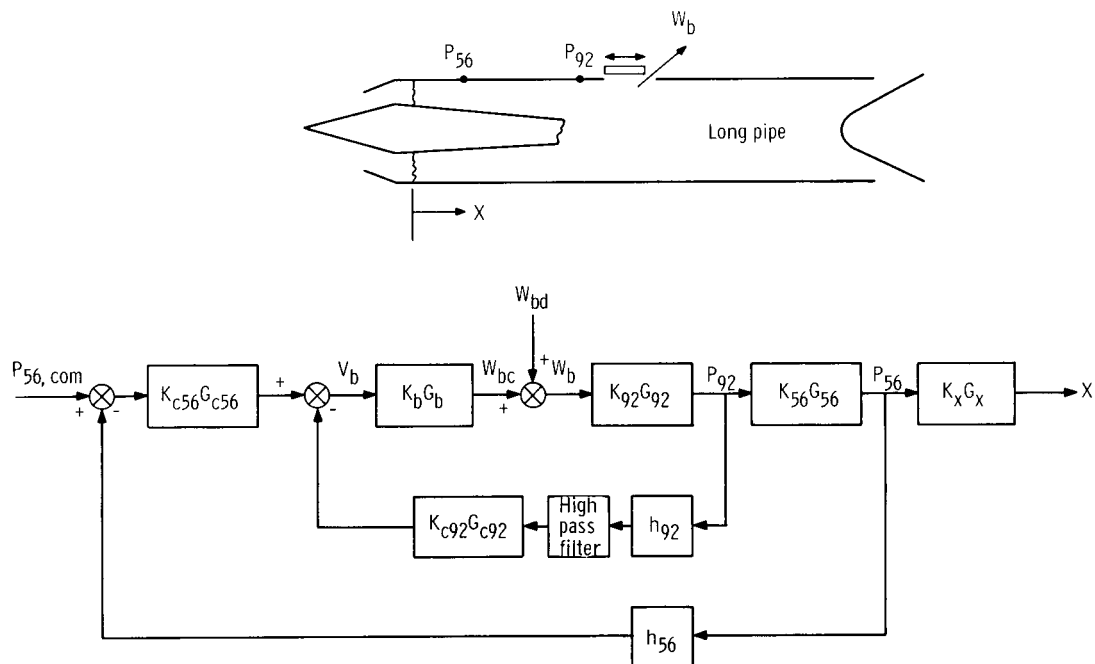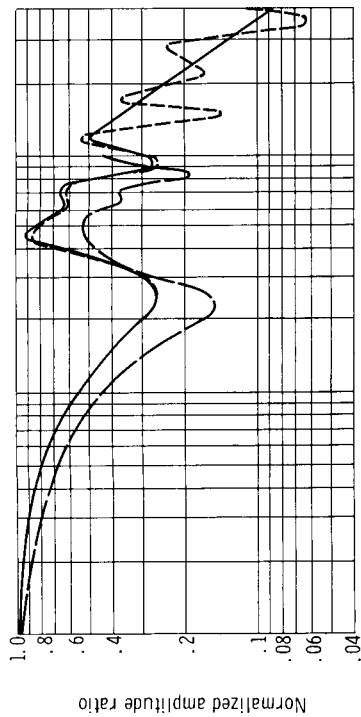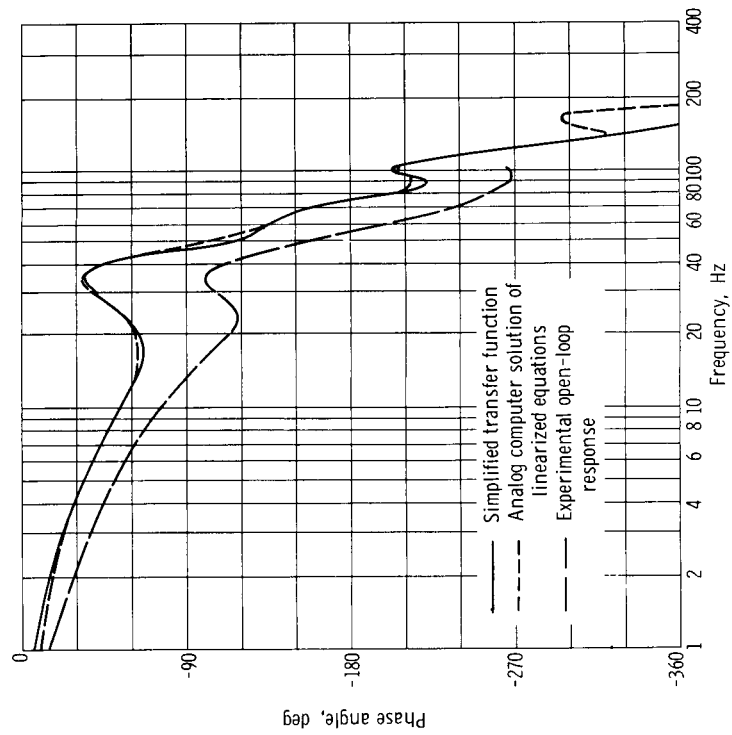

Figure 16. - Block diagram of inlet control for downstream airflow disturbances.
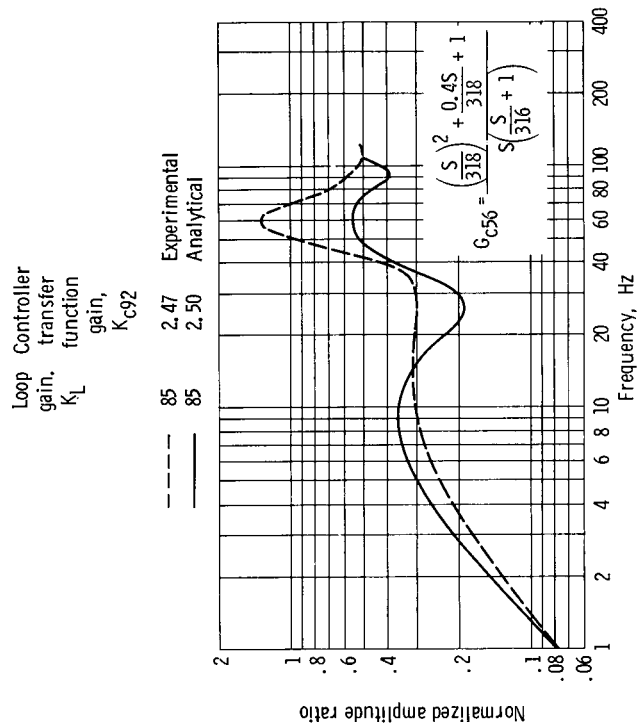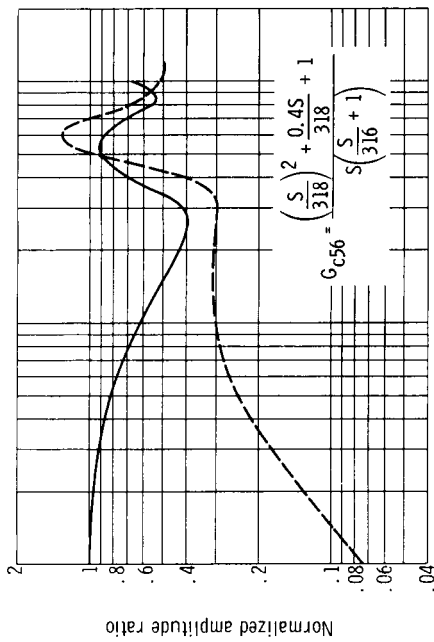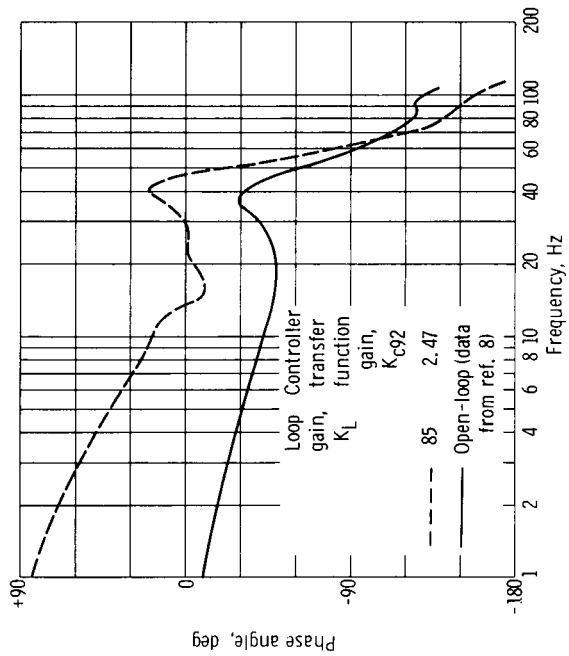
44

Figure 18. - Comparison of experimental $\Delta P_{56}/\Delta W_{bd}|_{CN}$ frequency response with analytical response using type 6 control. Inlet terminated with the long pipe; downstream airflow disturbance.
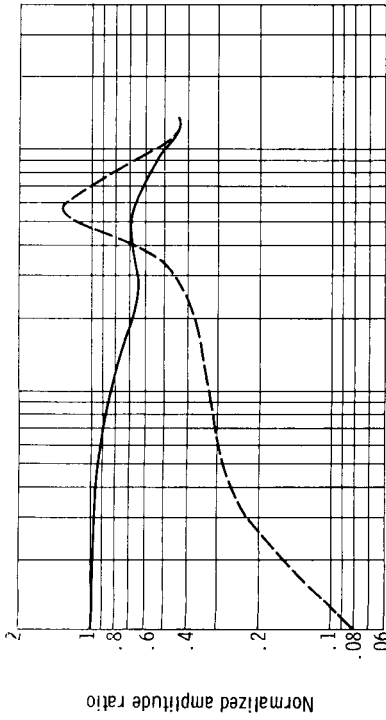
$$G_{c56} = \frac{\left(\frac{s}{318}\right)^2 + \frac{0.45 s}{318} + 1}{s\left(\frac{s}{316} + 1\right)}$$

Loop gain, K_L	Controller transfer function gain, K_{c92}	
85	2.47	Experimental
85	2.50	Analytical

Normalized amplitude ratio

Frequency, Hz

(a) Amplitude ratio.

Normalized amplitude ratio

(b) Phase angle.

Phase angle, deg

Frequency, Hz

Simplified transfer function

Analog computer solution of linearized equations

Experimental open-loop response

Figure 17. - Comparison of analytical and experimental open-loop frequency responses of X to W_{bd}.

45

(a) Amplitude ratio.

$$G_{C56} = \frac{\left(\frac{S}{318}\right)^2 + \frac{0.4S}{318} + 1}{S\left(\frac{S}{316} + 1\right)}$$

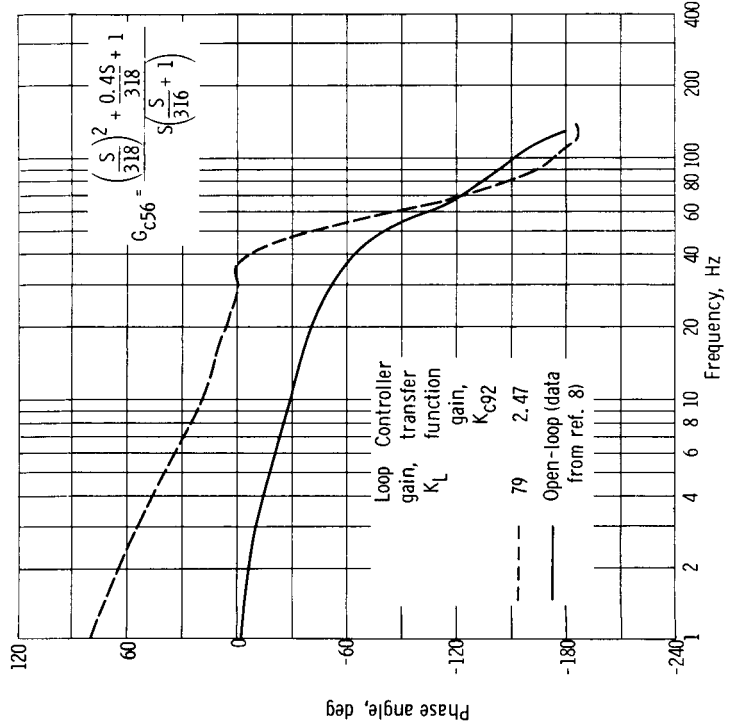| Loop gain, K_L	Controller transfer function gain, K_{C92}
– – – 79	2.47
—— Open-loop (data from ref. 8)	

(b) Phase angle.

Figure 20. – Comparison of experimental $\Delta P_{56}/\Delta W_{bd}$ frequency response for open-loop (no control) with that for type 6 control. Inlet terminated with choked orifice plate; downstream airflow disturbance.

(a) Amplitude ratio.

$$G_{C56} = \frac{\left(\frac{S}{318}\right)^2 + \frac{0.4S}{318} + 1}{S\left(\frac{S}{316} + 1\right)}$$

Loop gain, K_L	Controller transfer function gain, K_{C92}
– – – 85	2.47
—— Open-loop (data from ref. 8)	

(b) Phase angle.

Figure 19. – Comparison of experimental $\Delta P_{56}/\Delta W_{bd}$ frequency response for open-loop (no control) with that for type 6 control. Inlet terminated with long pipe; downstream airflow disturbance.
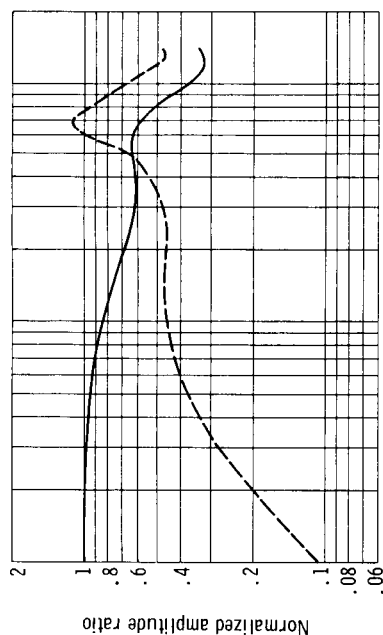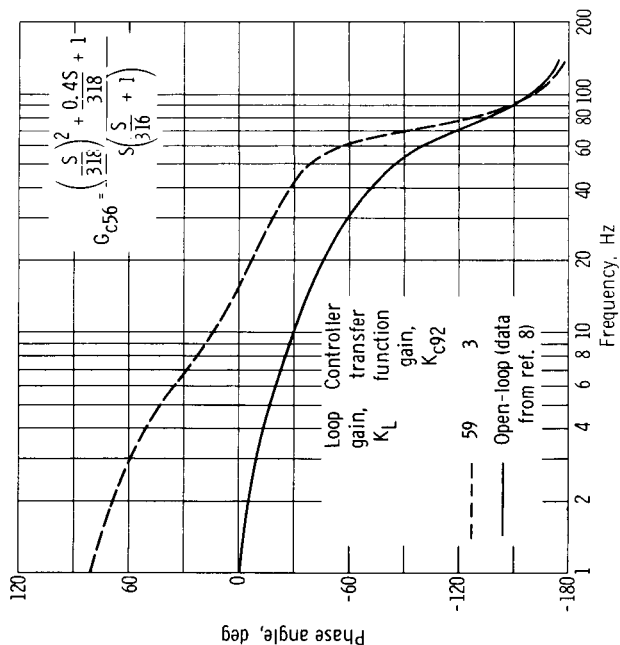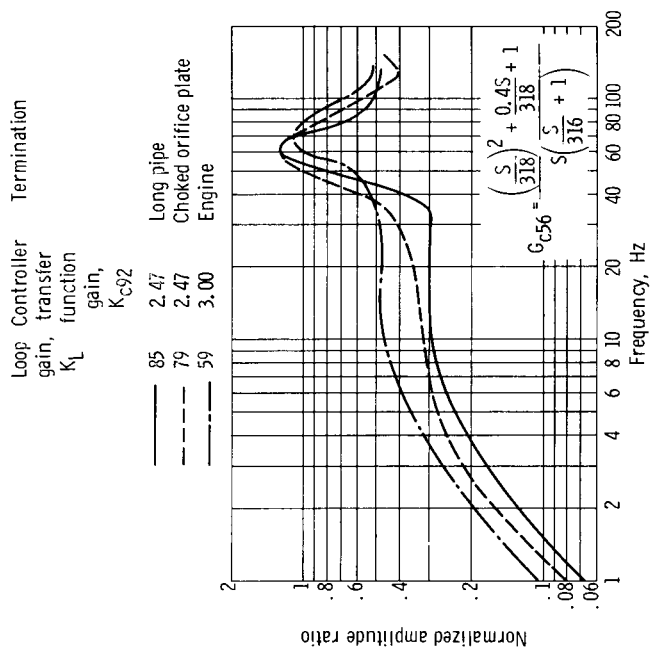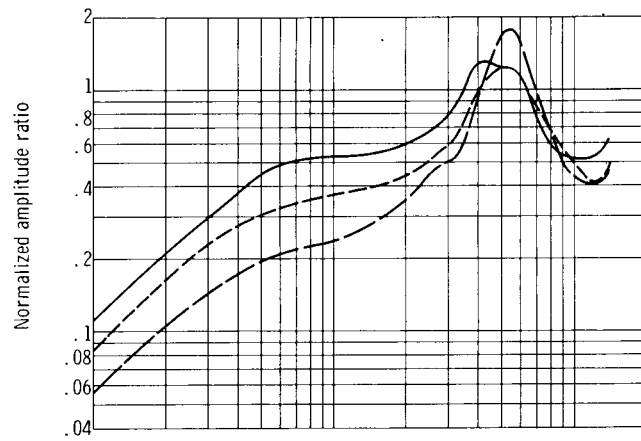
46

Figure 22. - Comparison of experimental $\Delta P_{56}/\Delta W_{bd}|_{CN}$ frequency responses showing effect of inlet termination for type 6 control; inlet subjected to downstream airflow disturbance.

$$G_{c56} = \frac{\left(\frac{S}{318}\right)^2 + \frac{0.4S}{318} + 1}{S\left(\frac{S}{316} + 1\right)}$$

Loop gain, K_L	Controller transfer function gain, K_{c92}	Termination
85	2.47	Long pipe
79	2.47	Choked orifice plate
59	3.00	Engine

(a) Amplitude ratio.

(b) Phase angle.

Figure 21. - Comparison of experimental $\Delta P_{56}/\Delta W_{bd}$ frequency response for open-loop (no control) with that for type 6 control. Inlet terminated with engine; downstream airflow disturbance.
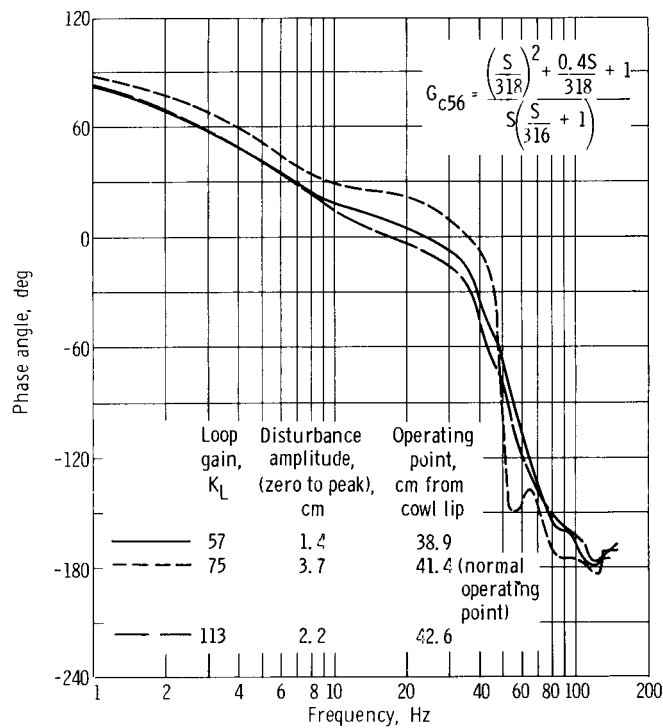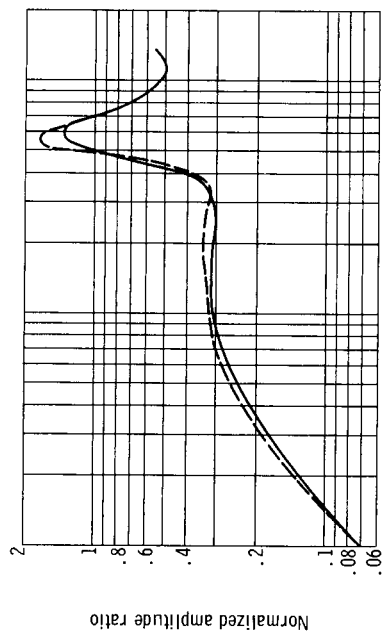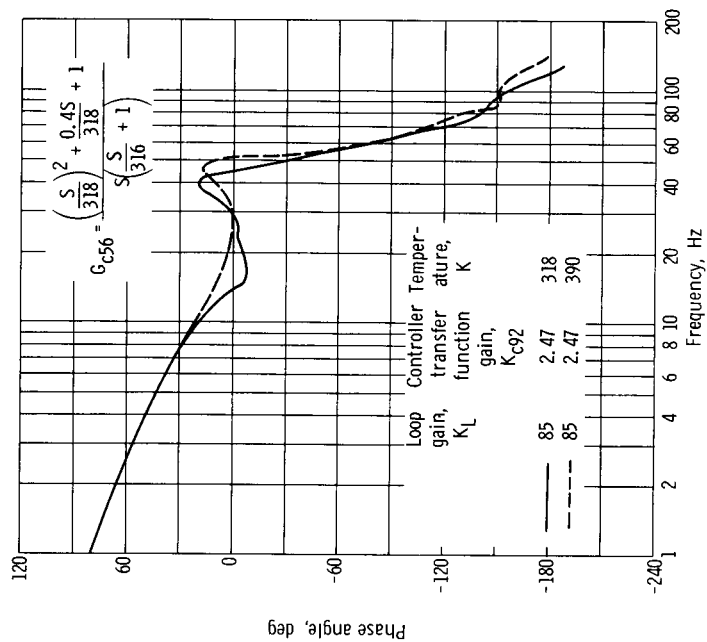
$$G_{c56} = \frac{\left(\frac{S}{318}\right)^2 + \frac{0.4S}{318} + 1}{S\left(\frac{S}{316} + 1\right)}$$

Loop gain, K_L	Controller transfer function gain, K_{c92}
59	3
Open-loop (data from ref. 8)	

47

(a) Amplitude ratio.

$$G_{c56} = \frac{\left(\frac{S}{318}\right)^2 + \frac{0.4S}{318} + 1}{S\left(\frac{S}{316} + 1\right)}$$

Loop gain, K_L	Disturbance amplitude, (zero to peak), cm	Operating point, cm from cowl lip
—— 57	1.4	38.9
— — — 75	3.7	41.4 (normal operating point)
— · — 113	2.2	42.6

(b) Phase angle.

Figure 23. - Experimental $\Delta P_{56}/\Delta W_{bd}|_{CN}$ frequency responses showing effect of varying operating point and disturbance amplitude on frequency response for type 6 control. Inlet terminated with choked orifice plate; downstream airflow disturbance. Controller transfer function gain, K_{c92}, 2.75.

(a) Amplitude ratio.

$$G_{C56} = \frac{\left(\frac{S}{318}\right)^2 + \frac{0.4S}{318} + 1}{S\left(\frac{S}{316} + 1\right)}$$

Loop gain, K_L	Controller transfer function gain, K_{C92}	Temperature, K
——— 85	2.47	318
- - - 85	2.47	390

(b) Phase angle, deg.

Figure 25. - Experimental $\Delta P_{56}/\Delta W_{bd}|_{CN}$ frequency responses showing effect of varying total free-stream total temperature for type 6 control. Inlet t terminated with the long pipe; down-stream airflow disturbance.

Normalized amplitude ratio

Phase angle, deg

Aft operating point and peak-to-peak amplitude (higher loop gain)

Nominal operating point and peak-to-peak amplitude (nominal loop gain)

Forward operating point and peak-to-peak amplitude (lower loop gain)

Control bypass door position
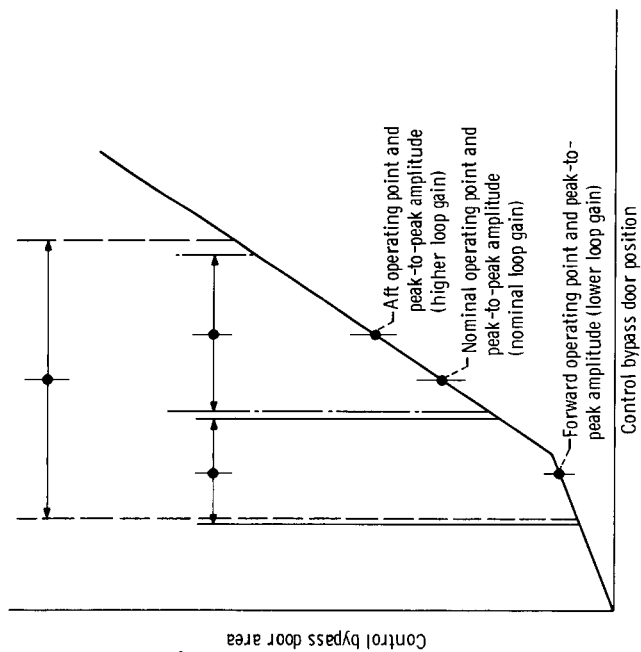
Figure 24. - Control bypass-door area as function of position showing different operating-point conditions and its effect on the loop gain.
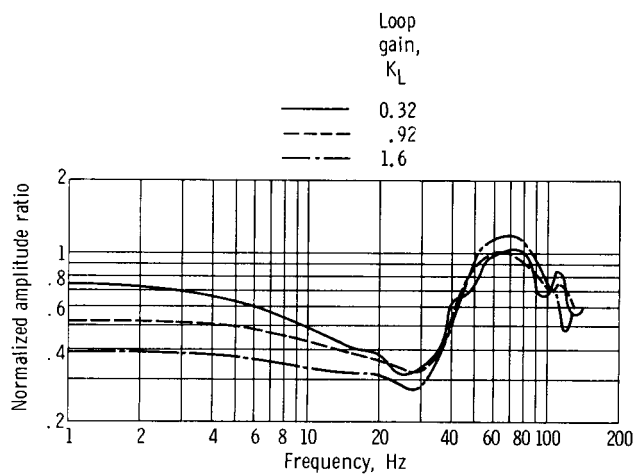
Control bypass door area

Figure 26. – Experimental $\Delta P_{92}/\Delta W_{bd}|_{CN}$ frequency response showing effect of varying controller gain for type 4 control. Inlet terminated with long pipe; downstream airflow disturbance.
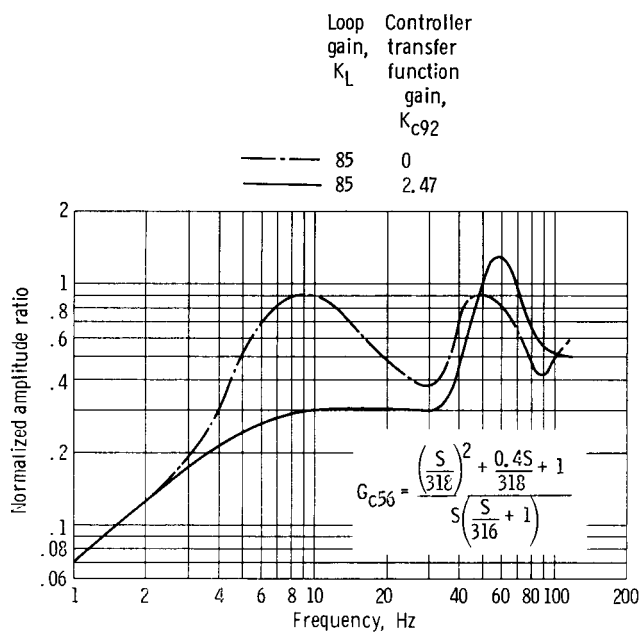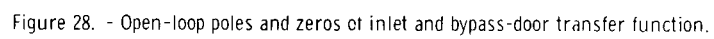

$$G_{c56} = \frac{\left(\dfrac{S}{318}\right)^2 + \dfrac{0.4S}{318} + 1}{S\left(\dfrac{S}{316} + 1\right)}$$

Figure 27. – Experimental $\Delta P_{56}/\Delta W_{bd}|_{CN}$ frequency responses showing effect of varying inner-loop gain K_{c92} for type 6 control. Inlet teminated with the long pipe; downstream airflow disturbance.
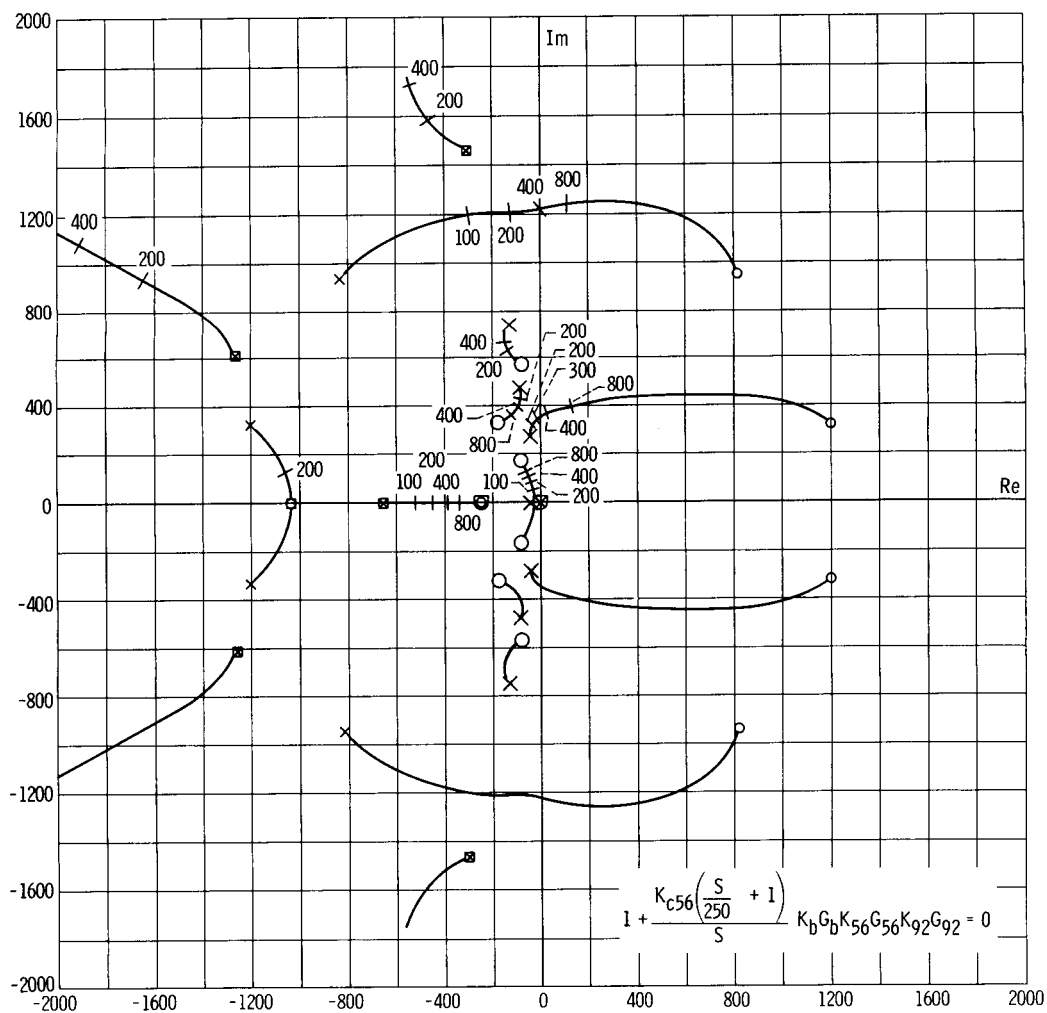
Figure 28. - Open-loop poles and zeros of inlet and bypass-door transfer function.

Figure 29. - Root locus for type 2 control.

The equation shown in the figure:

$$1 + \frac{K_{c56}\left(\frac{S}{250} + 1\right)}{S} K_b G_b K_{56} G_{56} K_{92} G_{92} = 0$$
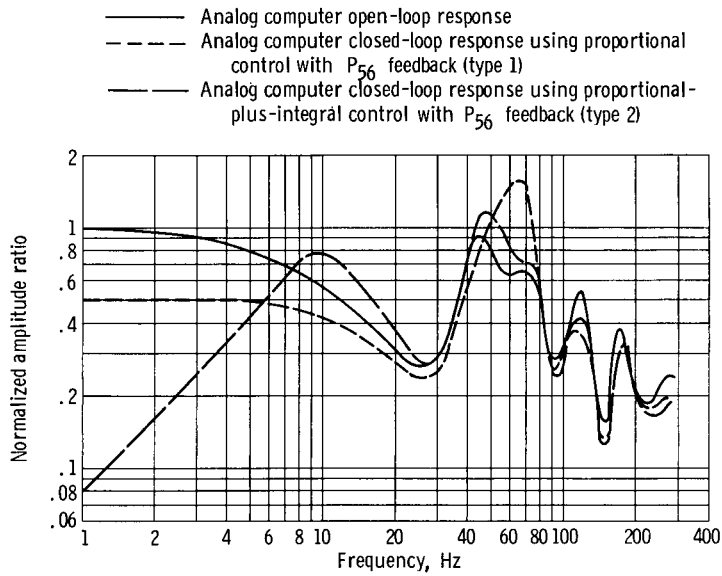
Figure 30. - Analytical $\Delta P_{56}/\Delta W_{bd}$ frequency responses using analog computer inlet simulation to obtain open-loop response and response using type 1 and 2 controls.
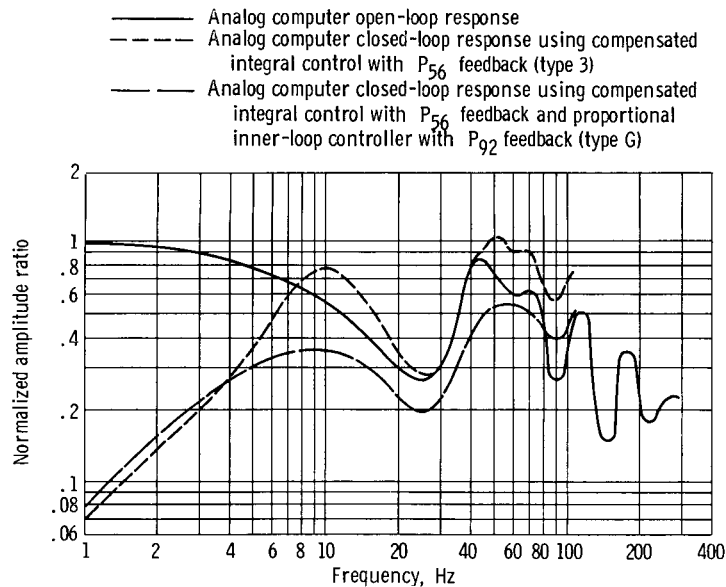

Figure 31. - Analytical $\Delta P_{56}/\Delta W_{bd}$ frequency responses using analog computer inlet simulation to obtain open-loop response and responses using type 3 and 6 controls.
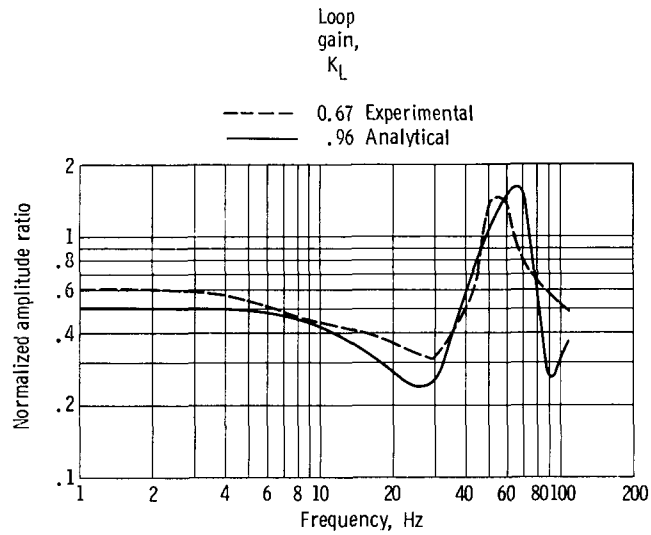
Loop
gain,
K_L

———— 0.67 Experimental
———— .96 Analytical

Figure 32. - Comparison of $\Delta P_{56}/\Delta W_{bd}|_{CN}$ experimental and analytical frequency responses of inlet using type 1 control. Inlet terminated with long pipe; downstream airflow disturbance.

———— Loop gain, 0.67
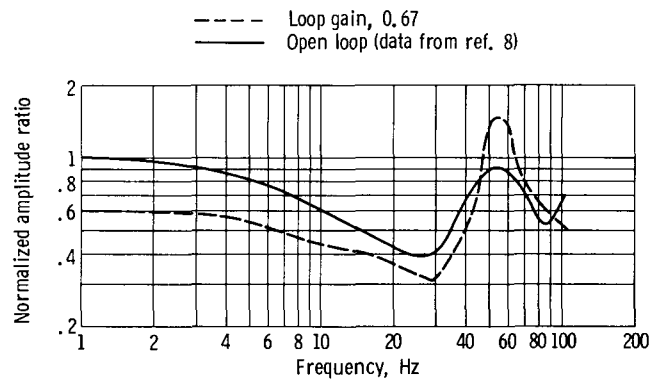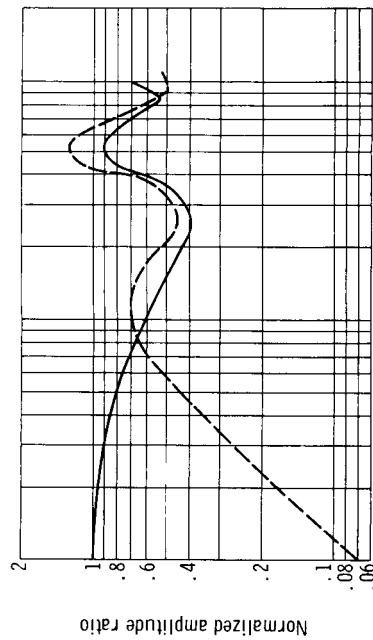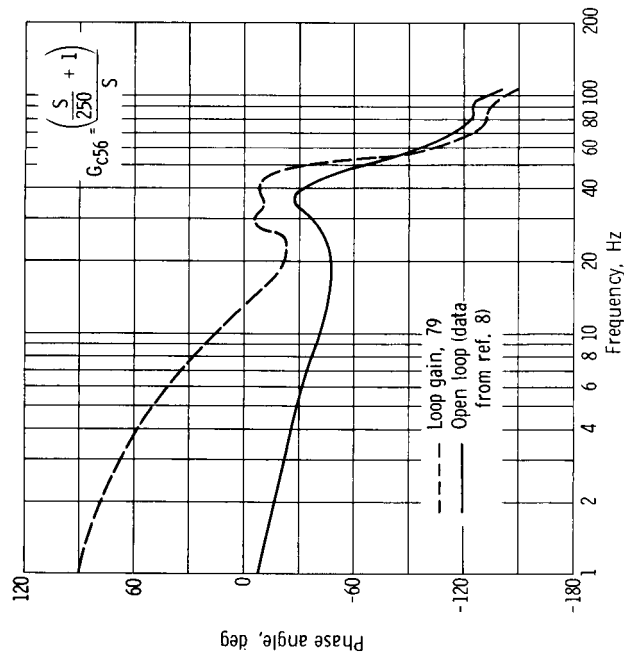———— Open loop (data from ref. 8)

Figure 33. - Comparison of experimental $\Delta P_{56}/\Delta W_{bd}$ open-loop frequency response with frequency response of inlet using type 1 control. Inlet terminated with long pipe; downstream airflow disturbance.

Experimental
Analytical

$G_{c56} = \left(\dfrac{\frac{S}{250} + 1}{S}\right)$

Normalized amplitude ratio

Frequency, Hz

Figure 35. - Comparison of $\Delta P_{56}/\Delta W_{bd}|_{CN}$ experimental and analytical frequency responses of inlet using type 2 control. Inlet terminated with long pipe; downstream airflow disturbance; loop gain, 79.

Normalized amplitude ratio

(a) Amplitude ratio.

$G_{c56} = \left(\dfrac{\frac{S}{250} + 1}{S}\right)$

Loop gain, 79
Open loop (data from ref. 8)

Phase angle, deg

Frequency, Hz

(b) Phase angle.

Figure 34. - Comparison of experimental $\Delta P_{56}/\Delta W_{bd}$ open-loop frequency response with frequency response of inlet using type 2 control. Inlet terminated with long pipe; downstream airflow disturbance.
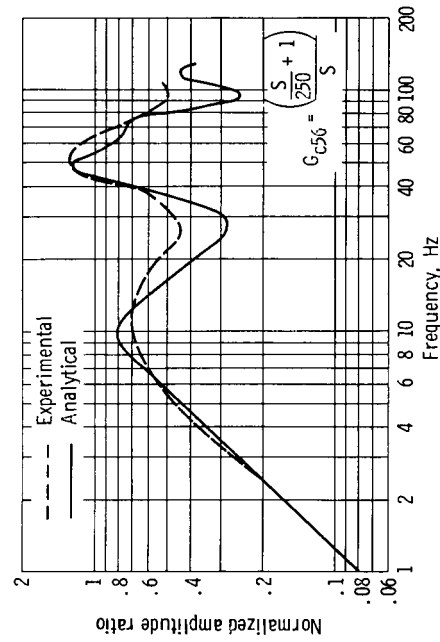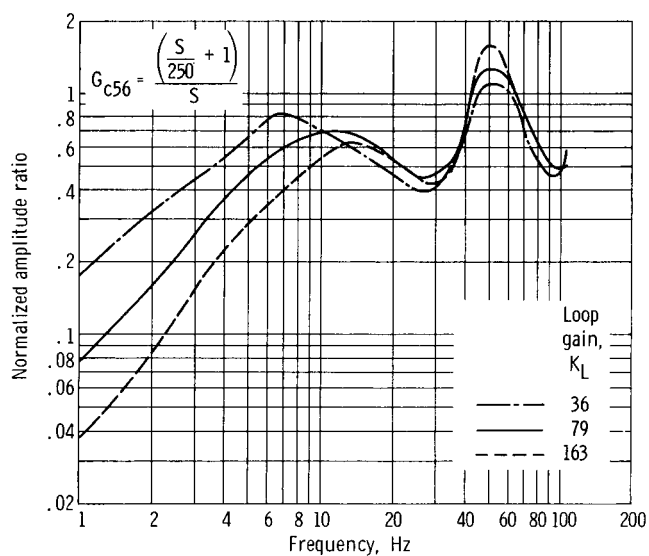
55

Figure 36. - Experimental $\Delta P_{56}/\Delta W_{bd}|_{CN}$ frequency responses of inlet showing effect of varying controller gain using type 2 control. Inlet terminated with long pipe; downstream airflow disturbance.
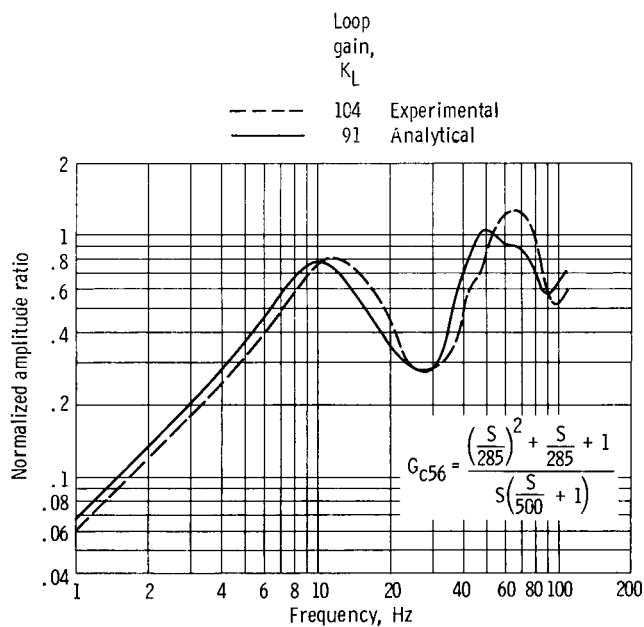
$$G_{c56} = \frac{\left(\frac{S}{250} + 1\right)}{S}$$

Figure 37. - Comparison of $\Delta P_{56}/\Delta W_{bd}|_{CN}$ experimental and analytical frequency responses of inlet using type 3 control. Inlet terminated with long pipe; downstream airflow disturbance.

$$G_{c56} = \frac{\left(\frac{S}{285}\right)^2 + \frac{S}{285} + 1}{S\left(\frac{S}{500} + 1\right)}$$

56

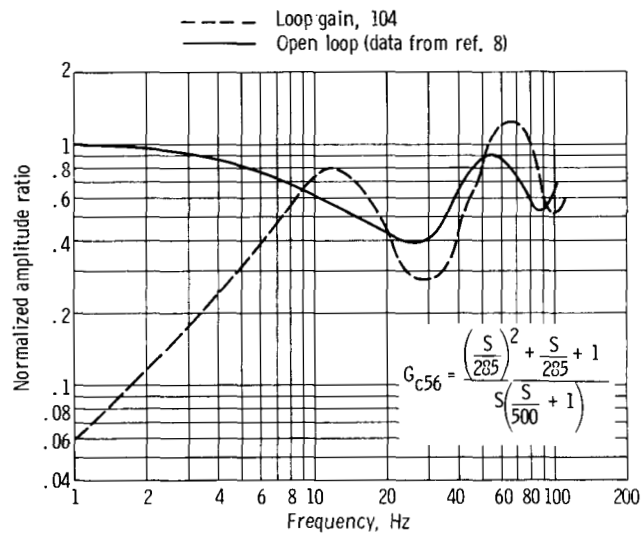$$G_{c56} = \frac{\left(\frac{S}{285}\right)^2 + \frac{S}{285} + 1}{S\left(\frac{S}{500} + 1\right)}$$

Figure 38. – Comparison of experimental $\Delta P_{56}/\Delta W_{bd}$ open-loop frequency response with frequency response of inlet using type 3 control. Inlet terminated with long pipe; downstream airflow disturbance.
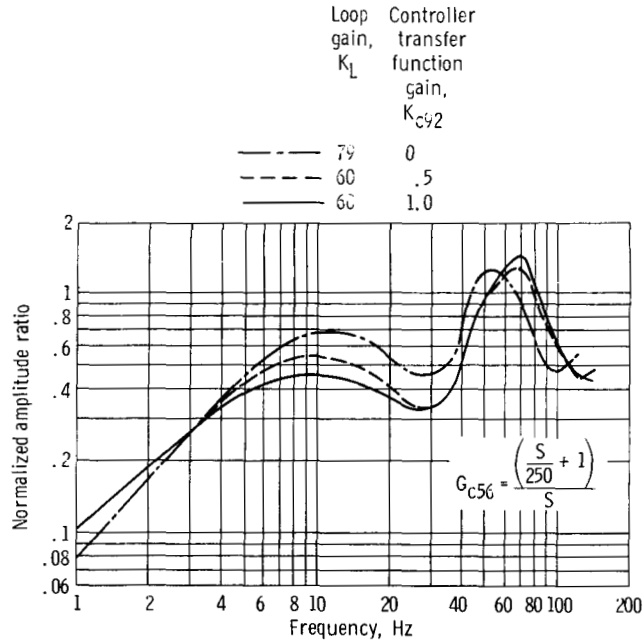
Loop gain, K_L	Controller transfer function gain, K_{c92}
79	0
60	.5
60	1.0

$$G_{c56} = \frac{\left(\frac{S}{250} + 1\right)}{S}$$

Figure 39. – Experimental $\Delta P_{56}/\Delta W_{bd}|_{CN}$ frequency responses of inlet showing effect of varying inner- and outer-loop controller gains using type 5 control. Inlet terminated with long pipe; downstream airflow disturbance.
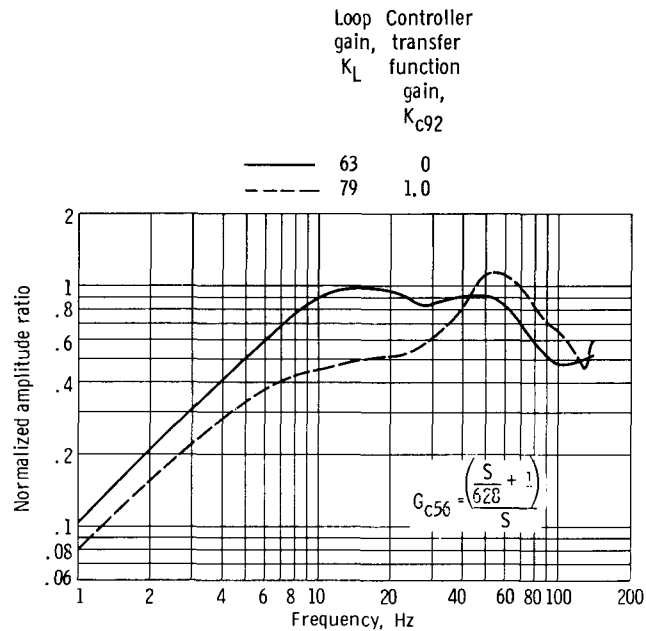
Loop   Controller
gain,   transfer
K_L function
gain,
K_{c92}

─────── 63   0
─ ─ ─ ─ 79   1.0

Figure 40. – Experimental $\Delta P_{56}/\Delta W_{bd}|_{CN}$ frequency responses of inlet showing effect of varying inner- and outer-loop controller gains using type 5 control. Inlet terminated with choked orifice plate; downstream airflow disturbance.
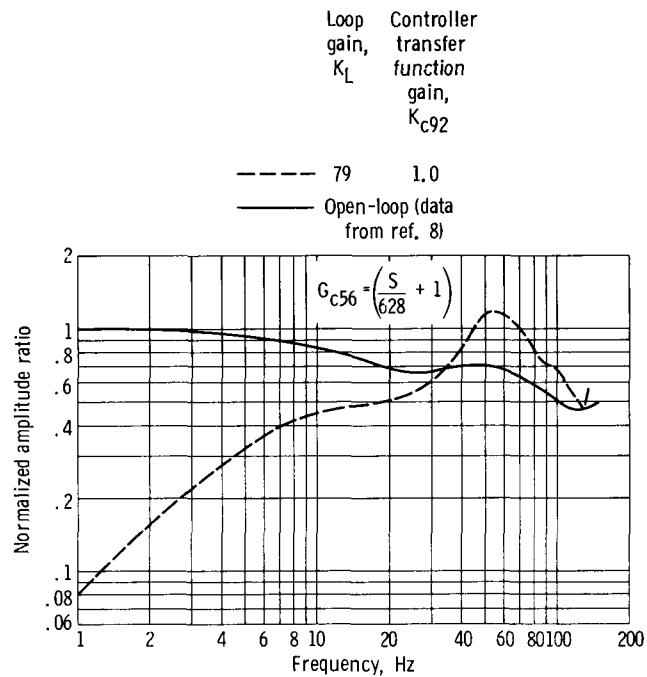
Loop   Controller
gain,   transfer
K_L function
gain,
K_{c92}

─ ─ ─ ─ 79   1.0
─────── Open-loop (data
from ref. 8)

Figure 41. – Comparison of experimental $\Delta P_{56}/\Delta W_{bd}$ open-loop frequency response with frequency response of inlet using type 5 control. Inlet terminated with choked orifice plate; downstream airflow disturbance.
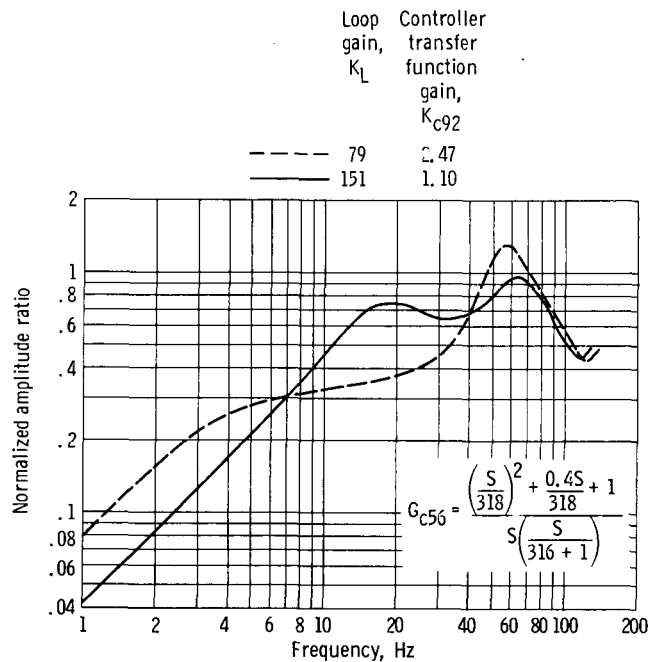
Loop gain, K_L	Controller transfer function gain, K_{c92}
———— 79	0.47
———— 151	1.10

$$G_{c56} = \frac{\left(\frac{S}{318}\right)^2 + \frac{0.4S}{318} + 1}{S\left(\frac{S}{316} + 1\right)}$$

Figure 42. - Experimental $\Delta P_{56}/\Delta W_{bd}|_{CN}$ frequency responses of inlet showing effect of varying inner- and outer-loop controller gains using type 6 control. Inlet terminated with choked orifice plate; downstream airflow disturbance.
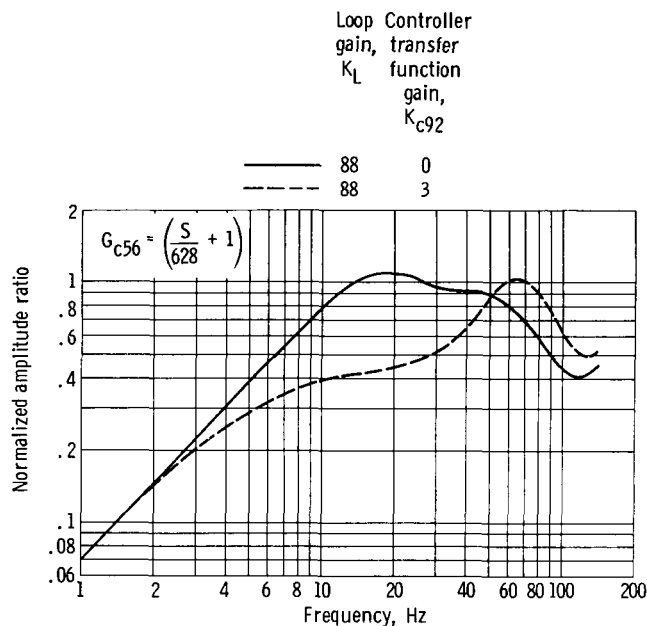

Loop gain, K_L	Controller transfer function gain, K_{c92}
———— 88	0
———— 88	3

$$G_{c56} = \left(\frac{S}{628} + 1\right)$$

Figure 43. - Experimental $\Delta P_{56}/\Delta W_{bd}|_{CN}$ frequency responses of inlet showing effect of varying inner-loop controller gain using type 5 control. Inlet terminated with engine; downstream airflow disturbance.

59

Loop   Controller
gain,   transfer
K_L function
gain,
K_{c92}

$- - - -$ 88   3

$--------$ Open-loop (data
from ref. 8)
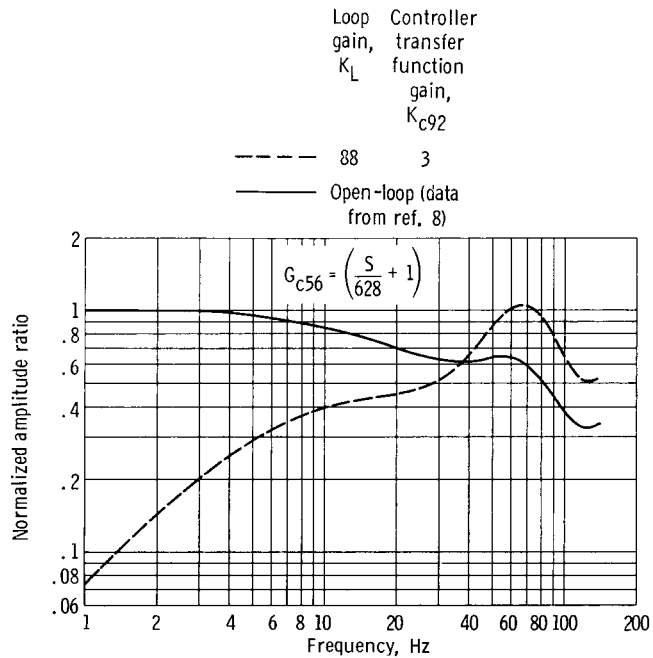
$$G_{c56} = \left(\frac{S}{628} + 1\right)$$

Figure 44. - Comparison of experimental $\Delta P_{56}/\Delta W_{bd}$ open-loop frequency response with frequency response of inlet using type 5 control. Inlet terminated with engine; downstream airflow disturbance.
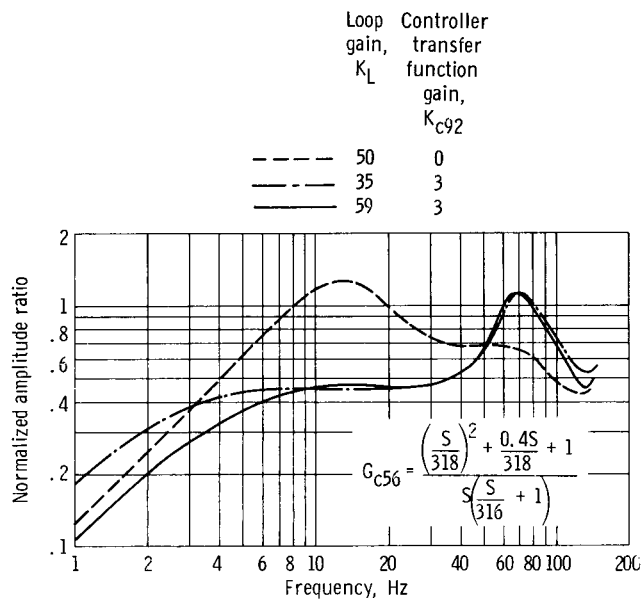
Loop   Controller
gain,   transfer
K_L function
gain,
K_{c92}

$- - - -$ 50   0

$-\cdot-\cdot-$ 35   3

$--------$ 59   3

$$G_{c56} = \frac{\left(\frac{S}{318}\right)^2 + \frac{0.4S}{318} + 1}{S\left(\frac{S}{316} + 1\right)}$$

Figure 45. - Experimental $\Delta P_{56}/\Delta W_{bd}|_{CN}$ frequency responses of inlet showing effect of varying inner- and outer-loop controller gains using type 6 control. Inlet terminated with engine; downstream airflow disturbance.

60

1. Report No. NASA TN D-6382	2. Government Accession No.	3. Recipient's Catalog No.
4. Title and Subtitle EXPERIMENTAL AND ANALYTICAL INVESTIGATION OF FAST NORMAL SHOCK POSITION CONTROLS FOR A MACH 2.5 MIXED-COMPRESSION INLET		5. Report Date July 1971
		6. Performing Organization Code
7. Author(s) George H. Neiner, Michael J. Crosby, and Gary L. Cole		8. Performing Organization Report No. E-5932
		10. Work Unit No. 720-03
9. Performing Organization Name and Address Lewis Research Center National Aeronautics and Space Administration Cleveland, Ohio 44135		11. Contract or Grant No.
		13. Type of Report and Period Covered Technical Note
12. Sponsoring Agency Name and Address National Aeronautics and Space Administration Washington, D.C. 20546		14. Sponsoring Agency Code

15. Supplementary Notes

16. Abstract

Simulation and experimental results are presented for several normal shock control systems using high-response (110-Hz bandwidth) overboard bypass doors. To date such control systems have used slower bypass doors (of the order of 10-Hz bandwidth). The best control, using two feedback loops and electronic compensation reduced shock motion below that without control for sinusoidal downstream airflow disturbances of up to 40 hertz. Inherent inlet dynamics constituted the main limitation on system closed-loop performance. Closed-loop control was demonstrated with the inlet terminated alternately with a long pipe, a choked orifice plate close to the diffuser exit station, and a J85-13 turbojet engine.

17. Key Words (Suggested by Author(s))	18. Distribution Statement Unclassified - unlimited		
19. Security Classif. (of this report) Unclassified	20. Security Classif. (of this page) Unclassified	21. No. of Pages 63	22. Price* $3.00